https://doi.org/10.5194/egusphere-2026-222
Preprint. Discussion started: 22 January 2026

Carbon flux responses to seasonal and annual hydroclimatic variability in a tropical dry forest in South Ecuador

Charuta Murkute[1], Franz Pucha-Cofrep[2], Galo Carrillo-Rojas[3], Jürgen Homeier[4,5], Oliver Limberger[6], Andreas Fries[2], Jörg Bendix[6], and Katja Trachte[1]

[1] Department of Atmospheric Processes, Brandenburg University of Technology Cottbus-Senftenberg, Burger Chaussee 2, 03046 Cottbus, Germany
[2] Hydrology and Climatology Working Group, Departamento de Ingeniería Civil, Universidad Técnica Particular de Loja, San Cayetano Alto, C. París, Loja 110107, Ecuador
[3] Departamento de Recursos Hídricos y Ciencias Ambientales, Facultad de Ciencias Químicas, Universidad de Cuenca, Av. Víctor Manuel Albornoz y los Cerezos, Cuenca 010107, Ecuador
[4] Faculty of Resource Management, HAWK University of Applied Sciences and Arts, Daimlerstraße 2, 37075 Göttingen, Germany
[5] Conservation Ecology, Department of Biology, University of Marburg, Karl-von-Frisch-Straße 8, 35032 Marburg, Germany
[6] Laboratory for Climatology and Remote Sensing, Department of Geography, University of Marburg, Deutschhausstrasse 12, 35032 Marburg, Germany

Correspondence: Charuta Murkute (murkute@b-tu.de)

Abstract. Tropical dry forests play an important role in the global carbon cycle, but their responses to climate variability are still not well understood. Using a three-year period (April 2022 to March 2025) of eddy covariance measurements, we studied seasonal and annual controls on carbon balances in a Tumbesian dry forest in Southern Ecuador. During the study period, the forest functioned as a net carbon sink, with a net ecosystem exchange (NEE) of -285 $gCm^{-2}year^{-1}$. The strongest carbon uptake occurred during the wet period (Feb - May) with 173.86 $\pm$ 66 $gCm^{-2}month^{-1}$, while it was reduced to 39.80 $\pm$ 8.12 $gCm^{-2}month^{-1}$ in the dry season (August - November).

Light use efficiency (LUE) and water use efficiency (WUE) were used to characterize the functional controls on carbon fluxes at both seasonal and annual scales. WUE showed relatively stable water–carbon exchange, whereas LUE displayed clear seasonal variation, reflecting the strong influence of seasonal vegetation growth and greenness. Principle component analysis (PCA) was conducted to further analyze controlling mechanisms in carbon fluxes. Seasonal results showed that gross primary productivity (GPP) was mainly controlled by energy-related factors, while ecosystem respiration (Reco) was primarily driven by a moisture–temperature gradient. Annually, GPP was predominantly influenced by variations in vapor pressure deficit (VPD), soil temperature (Ts), and incoming radiation (Rg), reflecting a strong coupling between surface energy balance and atmospheric moisture demand. These drivers were further modulated by ENSO related climate variability, as reflected by shifts in their PCA loadings across years. Overall, the results reveal a decoupling between photosynthesis and respiration and show that tropical dry forests are highly vulnerable to increasing climate extremes, highlighting the need for improved representation of these processes in Earth system models.

https://doi.org/10.5194/egusphere-2026-222
Preprint. Discussion started: 22 January 2026

1 Introduction

Tropical dry forests are among the most threatened biomes due to global change Siyum (2020). They cover approximately 42% of tropical forest areas and play a key role in carbon storage, regulating regional climate and conserving biodiversity Miles et al. (2006); Portillo-Quintero and Sánchez-Azofeifa (2010). Due to the moderate annual carbon assimilation, but low mean respiration of this semi-arid ecosystems, dry forests are highly efficient carbon sequesters Poulter et al. (2014). However, dry forests remain one of the most understudied tropical ecosystems, particularly in the context of climate change and their role in the global carbon cycle Brienen et al. (2015); Ahlström et al. (2015). In recent years they are increasingly recognized as important carbon sinks due to their capacity to sequester atmospheric CO_2, especially through slow-growing hardwood species adapted to drought conditions Bennett et al. (2023).

In general, tropical dry forests are shaped by precipitation, temperature and soil moisture (SM) availability Rojas-Robles et al. (2020); González-Jaramillo et al. (2016); Rodda et al. (2021); Stan and Sanchez-Azofeifa (2019). The precipitation regimes are related to seasonal circulation systems, which induce distinct wet and dry periods. In the tropical montane dry forest located in the Andes Mountains of South Ecuador, these eco-hydrological dynamics are particularly driven by the interplay between topography and mesoscale circulation patterns Garreaud et al. (2009) controlling the atmospheric moisture transport pathways Trachte (2018). Moreover, macroscale El Nino Southern Oscillation (ENSO) dynamics significantly influence precipitation patterns with feedback to the seasonal cycle Rollenbeck et al. (2022); Spannl et al. (2016). The seasonal availability of water strongly further affects the net carbon balance and plays a crucial role in the phenological cycle Mendes et al. (2025); Rollenbeck et al. (2022). During the rainy season, rapid leaf development enhances photosynthetic capacity and gross primary production (GPP). In contrast, the dry season is marked by water stress in terms of low soil moisture (SM) and high vapor pressure deficit (VPD), leaf senescence, and reduced microbial and root activity, leading to a sharp decline in carbon uptake.

The seasonal dynamic is clearly reflected in the carbon patterns observed in tropical dry forests worldwide. In Mexican old-growth forests, the mean GPP during the wet season reached 1601.4 $gCm^{-2}year^{-1}$ but declined to only 373.3 $gCm^{-2}year^{-1}$ in the dry season Rojas-Robles et al. (2020). These patterns are primarily driven by changes in canopy leaf density and SM Rodda et al. (2021). Similarly, in the Caatinga biome in Brazil, high carbon-use efficiency was observed even during years with shortened rainy seasons, with phenological responses closely tied to water availability Castro et al. (2018). In the dry forests of India and Argentina, temperature and SM emerge as dominant controls of CO_2 fluxes depending on seasonal and site-specific conditions García et al. (2017).

Additionally, further studies have also shown that different environmental factors are prioritized to shape the carbon balances. Humphrey et al. (2021) demonstrated that the terrestrial carbon uptake was mainly driven by SM, while Wu et al. (2021) pointed to global radiation for tropical evergreen forests and Novick et al. (2024) to VPD as an important climatic factor for the carbon cycle in natural and managed ecosystems. This underpins the importance of regional characteristics in carbon exchange between vegetation and the atmosphere. Although recent studies have advanced our understanding of carbon dynamics in lowland tropical dry forests, highlighting the sensitivity of carbon exchange to climatic variability (e.g., Mendes et al. (2020)), information from montane sites remains scarce. Furthermore carbon accumulation dynamics during post dry season refoliation

https://doi.org/10.5194/egusphere-2026-222
Preprint. Discussion started: 22 January 2026

and the effects of climatic events in tropical dry forests remain poorly understood Calvo-Rodriguez et al. (2021) due to limitation of in-situ measurements, which makes it difficult to draw robust conclusions about their long-term carbon storage potential Ahlström et al. (2015); Biederman et al. (2016). As shown by Ahlström et al. (2015), the variability of carbon uptake is related to distinct biogeographic regions. The authors highlighted that semi-arid ecosystems play an important role in driving trends and interannual variations in the global carbon cycle, primarily due to seasonal water availability, which was further supported by Biederman et al. (2016).

In light of these findings, concerns are growing about the potential impacts of climate change on tropical dry forests, where projected shifts in rainfall patterns are expected to reduce overall precipitation and intensify dry periods Castro et al. (2018). At the same time, montane regions are particularly vulnerable to accelerating warming trends Vuille et al. (2015). Thus, knowledge about carbon exchange over tropical montane forests and the influence of climatic factors is highly needed. This will advance our understanding of regional and global carbon dynamics essential, which is essential to improve future climate predictions, as well as to strengthen carbon mitigation strategies (Rodda et al., 2021; Wang et al., 2022).

In order to obtain detailed information on water and carbon exchanges, the eddy covariance (EC) measurement technique provides valuable observations at the ecosystem level Baldocchi (2003). This technique captures water and carbon fluxes, allowing the calculation of net ecosystem exchange (NEE), which represents net carbon uptake or release Loescher et al. (2003). Flux partitioning methods also allow for the estimation of GPP and ecosystem respiration (Reco) Papale et al. (2006); Reichstein et al. (2005). However, EC measurements in complex terrain present operational challenges due to horizontal and vertical variations in wind velocity and scalar fluxes, leading to advective fluxes that disrupt the energy balance closure (EBC) Turnipseed et al. (2004). These effects are particularly evident on calm, clear nights, when cold air drainage lowers nighttime temperatures and reduces ecosystem respiration Novick et al. (2013); Hammerle et al. (2007). Despite these challenges, previous studies in complex topography showed the applicability of EC measurements Xing et al. (2023); Hiller et al. (2008); Malhi et al. (1998); Del Castillo et al. (2018).

The objective of this study is to investigate the carbon balance of the Tumbesian dry forest in southern Ecuador to improve our understanding of carbon flux dynamics under varying climatic conditions. To achieve this, we used continuous EC measurements above the forest canopy over a three-year period to quantify the exchange of carbon and water fluxes. Specifically, the aims are (i) to analyze the seasonal and interannual variability of the carbon sink function and (ii) to assess the sensitivity of carbon fluxes to key environmental drivers. Due to few studies in tropical montane dry forests, the results will advance our understanding of carbon exchange processes and dynamics in semi-arid ecosystems, which will reduce uncertainties in simulations of local and global carbon cycling in land surface and atmospheric models.

2 Materials and Methods

2.1 Study Site

The study was carried out in the Reserva Natural Laipuna, located in southern Ecuador within the Tumbesian dry forest region on the western escarpment of the Andes Mountains Fig.1. This region is characterized by montane topography with altitudes

https://doi.org/10.5194/egusphere-2026-222
Preprint. Discussion started: 22 January 2026

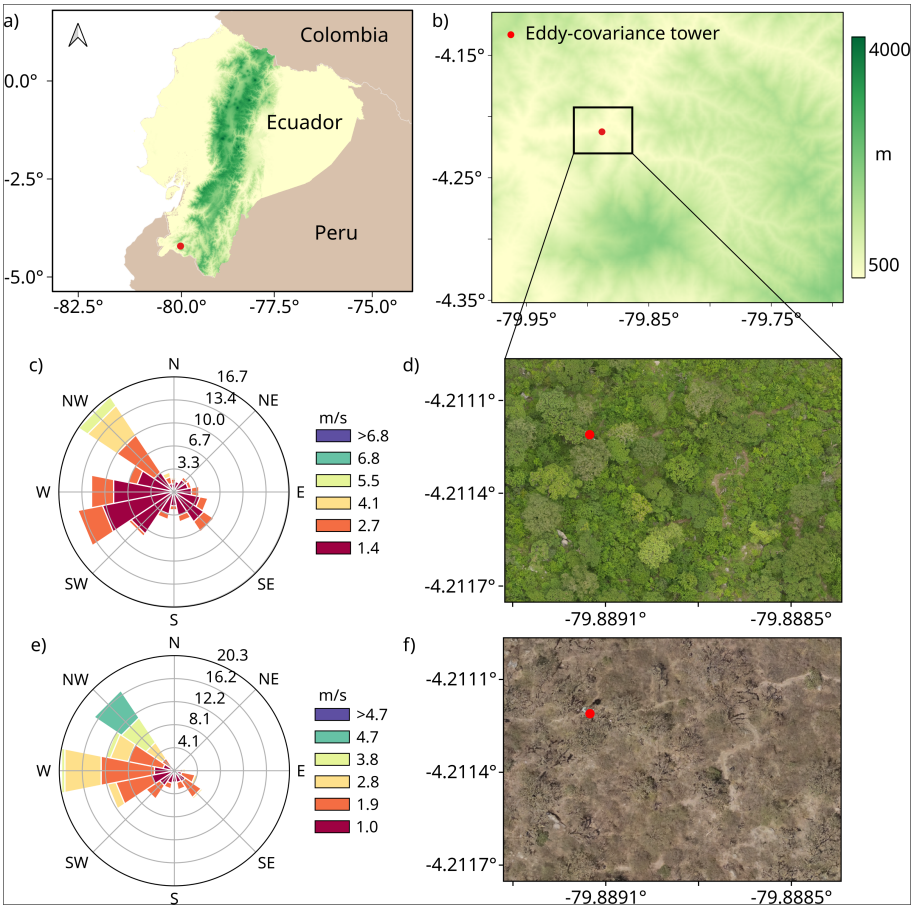

Figure 1. Study area and geographic location of the eddy-covariance flux tower a) map of Ecuador, b) location of the study site, (c, d) wind rose and study site during wet season and (e, f) wind rose and study site during dry season.

ranging from 600 to 1,450 m a.s.l. The underlying geology is dominated by acidic Cretaceous intrusive granitic bedrock, which has given rise to predominantly shallow, young, and weakly developed soils classified as Torriorthents. These soils are typically coarse textured, acidic, and well drained, resulting in general low soil fertility Spannl et al. (2016). Annual precipitation totals vary between 350 and 800 mm with high interannual variability (standard deviation $\pm$ 218 mm) due to the frequently occurring El Niño phenomenon Bendix et al. (2017). The region experiences a distinct dry season typically from June to December and a rainy season from January to May. During the wet season the moisture-laden air masses from the Pacific Ocean bring rain in form of convective clouds and thunderstorms Fries et al. (2014); Best and Kessler (1995). The seasonal climate variability in the region is driven by the meridional migration of the Intertropical Convergence Zone (ITCZ). When the ITCZ shifts southward, subsidence and relatively higher surface pressure dominate, suppressing cloud formation and rainfall Spannl et al. (2016); Pucha-Cofrep et al. (2015). In contrast, the passage of the ITCZ over the region is associated with lower surface pressure, atmospheric instability, and enhanced convection, resulting in increased precipitation.

https://doi.org/10.5194/egusphere-2026-222
Preprint. Discussion started: 22 January 2026

Precipitation affects all aspects of the forest in the Laipuna Reserve, which is of smaller stature and lower aboveground biomass compared to tropical rain forests at similar elevations Gonzalez-Valdiviezo et al. (2025); Werner and Homeier (2024). Deciduous woody components (tree, shrubs and lianas) are the most dominant plants at lower elevations of the study area, the number and abundance of semi-deciduous and evergreen species is increasing at higher elevation. Canopy height averages 11–16 m regardless of elevation, with the tallest individual trees reaching up to 20 m Werner and Homeier (2024).

2.2 Instrumentation

The EC flux tower was installed in April 2022 at the location -4.2116°S and -79.8891°E at an altitude of 702 m a.s.l. The system is installed at a height of 20 m with an average canopy height of 15 m. It consists of a 3D sonic anemometer and an open path infrared gas analyzer (IRGASON, Campbell Scientific) measuring with a frequency of 10 Hz. Net-radiation components are obtained using a net-radiometer (NR01, Hukseflux) and photosynthetic active radiation (PAR) is measured by the quantum sensor (SKP215, Skye Instruments). Additionally, air temperature (Ta) and relative humidity (RH) (VAISALA, HMP115) and precipitation (RM Young, Tipping Bucket rain gauge) are measured. At a depth of 10-20 cm SM and soil temperature (Ts) are observed by the TDR soil water sensor (CS655, Campbell Scientific). Ground heat flux (G) is obtained using the self-calibrating soil heat flux plate (HFP01-SC, Hukseflux). All variables are averaged to half-hourly intervals and stored in the data logger (CR6, Campbell Scientific). In order to quantify the contribution of soil CO_2 effluxes to total respiration (Reco), the Li-COR Inc. smart chamber (LI-870 CO_2/H_2O gas analyzer and 8200-01S Smart chamber) was used in field campaigns. Three collars were installed within the footprint of the EC tower to obtain replicate measurements. They were performed on a 15 minute interval.

2.3 Pre-processing and Quality Control

A two-phase quality control routine was carried out to ensure a good estimate of vertical fluxes that eliminates spurious data. The first phase was performed using the EddyPro 7.0.9 software. It included a series of standard corrections Foken et al. to ensure a better estimate of vertical fluxes while discarding outliers and correcting possible problems such as flow distortions insufficient turbulence under stable or nighttime conditions, leading to underestimated fluxes instrumental and setup errors such as sensor misalignment and frequency response losses. Corrections involve spike removal and raw data statistical screening Mauder et al. (2013); Vickers and Mahrt (1997), time lag compensation by covariance maximization Moore (1986), and correction for high-frequency spectral losses Foken et al. (2012). Due to the topography and heterogeneity of the canopy, the planer fit approach with 30° sectors was used Wilczak et al. (2001). Differences and air density fluctuations due to changes in temperature and water vapor were corrected according to Webb et al. (1980). We also calculated the random error of the original CO_2 fluxes according to the method reported by Finkelstein and Sims (2001). The footprint of the EC tower was estimated using the analytical model reported by Kljun et al. (2015).

In the second phase of the quality control outliers in the final calculated fluxes were eliminated based on a default statistical criterion, i.e. flux values ≤ 2 times the standard deviation of the whole dataset. Furthermore, fluxes under rainfall events and equipment failure were also removed. The primary step in the data quality control process involved spike detection using the

https://doi.org/10.5194/egusphere-2026-222
Preprint. Discussion started: 22 January 2026

Median Absolute Deviation (MAD) method Papale et al. (2006). Based on the filtering technique of Del Castillo et al. (2018), we filtered our data on dimensionless turbulent intensity indices I_u and I_w derived from the ratio of mean horizontal ($\overline{u}$) wind and estimated vertical ($\overline{w}$) wind velocities to turbulent kinetic energy u_{TKE} Wharton et al. (2009). They are defined as follows:

$$I_u = \frac{u}{u_{\text{TKE}}} \tag{1}$$

$$I_w = \frac{w_{\text{plane}}}{u_{\text{TKE}}} \tag{2}$$

The turbulence intensity scale u_{TKE} is defined as

$$u_{\text{TKE}} = \left(u'^2 + v'^2 + w'^2\right)^{\frac{1}{2}} \tag{3}$$

where u^2, v^2, and w^2 are the variances of the horizontal (u), crosswind (v), and vertical (w) wind velocities. The use of u_{TKE} assumes that the magnitude of turbulent kinetic energy (TKE) of the flow controls the efficiency of turbulence to transport mass and energy. In order to identify the conditions under which a significant contribution of advective transport of a scalar occurred.

$$I_u = \frac{u}{u_{\text{TKE}}} \tag{4}$$

$$I_w = \frac{w_{\text{plane}}}{u_{\text{TKE}}} \tag{5}$$

estimated through multiple regression of the measured ($\overline{w}$) on the mean horizontal components of wind velocity.

Paw U et al. (2000) and Wilczak et al. (2001): w = b + bu + bv, where b_0, b_1, and b_2 are the sector-specific multiple regression coefficients of the planar fit rotation. A critical value for each measure of turbulence strength was determined visually by inspecting a scatterplot of NEE versus a given filter for both daytime and nighttime given in Table 1. The filtering processes assume that the release and consumption of carbon through photosynthesis and respiration are independent of the intensity of turbulence. The use of dimensionless filters that are inversely proportional to the effectiveness of turbulent transport of mass and energy was effective in discriminating and eliminating periods when the vertical or horizontal advection cannot be neglected. We estimated I_u and I_w thresholds for different time periods for our analysis mentioned in table A1. The plots determined are also added in the supplementary material.

During nighttime, the atmospheric boundary layer is often weak or absent, resulting in an isothermal stratification of the air column that limits vertical mixing resulting in net ecosystem exchange (NEE) values unrepresentative of actual gas exchange in the ecosystem Wutzler et al. (2018); Loescher et al. (2003). Therefore, we used the R package Reddy Proc version 1.3.3 and the guide proposed by Wutzler et al. (2018), to select a critical friction velocity (u*) threshold to avoid systematic biases under

https://doi.org/10.5194/egusphere-2026-222
Preprint. Discussion started: 22 January 2026

calm wind conditions Papale et al. (2006). The u* threshold was seasonally calculated, resulting in a range of 0.13 to 0.25 ms^{-1} between seasons considering the differences in surface roughness due to changes in canopy phenology and the presence of rain events. The u* threshold was based on seasons divided into four periods dry (August-November), wet(February- May) , wet-to-dry (June and July) and dry-to-wet (December and January) Wutzler et al. (2018); Barr et al. (2013) and implementation of the moving point method. After all quality control procedures, the data available for analysis of NEE accounted for 73% in 2022–2023, 72% in 2023–2024, and 76% in 2024–2025. For consistency, the analysis period for all years was defined from (April to March).

2.4 Correction of Incoming Radiation

To account for the influence of slope and aspect on radiation measurements, corrections were applied to net radiation. Direct solar radiation was adjusted on the basis of the angle between the solar beam and the normal to the slope, which depends on the slope inclination, azimuth, and solar declination. A semi-empirical method developed by Matzinger et al. (2003) was used to estimate net radiation parallel to the slope by relating it to horizontally measured values using a proportional function. Since the study site had similar conditions to those described in Matzinger et al. (2003); Hiller et al. (2008), their regression parameters were adopted (a = 1.89 * 10^{-5}, b = 0.34). The solar declination was calculated using the algorithm of Whiteman et al. (1989). The detailed method is provided in Murkute et al. (2024).

2.5 Energy Balance Closure

The EBC is essential for accurately quantifying the exchange of energy between the land surface and the atmosphere Foken et al. (2012). It represents the conservation of energy at the surface and is defined as

$$R_n = H + LE + G + \epsilon \tag{6}$$

with R_n representing net radiation, H the sensible heat flux, LE the latent heat flux, G the ground heat flux and ϵ indicates the closure error term, accounting for residuals arising from inaccuracies in the measured fluxes.

In the EBC ϵ should be minimal ensuring that all significant energy fluxes are accurately measured. This is particularly challenging in complex terrains where slope, aspect, and surface orientation impact incident radiation. Such conditions can cause discrepancies in R_n due to directional effects on incoming solar radiation. To improve the accuracy of the energy balance on sloped or uneven terrain, we used the corrected net radiation ($R_{n\psi}$), which adjusts R_n for surface-normal conditions. This correction accounts for the slope angle, the aspect, and the position of the sun by calculating the modified global irradiance ($R_{g\psi}$) which is then used to derive $R_{n\psi}$. The adapted energy balance equation is

$$R_{n\psi} = H + LE + G + \epsilon \tag{7}$$

https://doi.org/10.5194/egusphere-2026-222
Preprint. Discussion started: 22 January 2026

2.6 Functional relationships

In order to estimate the functional relationships of water and light with carbon uptake, water use efficiency (WUE) and light use efficiency (LUE) are calculated. Both metrics provide valuable information on the efficiency of the dry forest in using the environmental conditions for carbon assimilation. WUE is a critical metric used to quantify the water utilization in relation to carbon assimilation in ecosystems. It is estimated as the ratio of GPP (gC m^{-2}) to evapotranspiration (ET, mm) representing the total carbon fixed by vegetation per water loss:

$$WUE = \frac{GPP}{ET} \tag{8}$$

LUE represents the efficiency of plants to convert light energy into biomass through carbon assimilation. It is defined as

$$LUE = \frac{GPP}{\text{PPFD}} \tag{9}$$

with PPFD as photosynthetic photon flux density (μmol m^{-2} s^{-1}) representing the incident light used for photosynthesis. which does not account for absorption efficiency. LUE is given in gC μmol^{-1}.

2.7 Vegetation state

To assess the greenness of the vegetation at the EC flux tower, we used the Normalized Difference Vegetation Index (NDVI) derived from the version 2 product, which is part of the Copernicus Global Land Service (CGLS). It provides high-resolution optical imagery with a spatial resolution of 300 meters Copernicus Global Land Service (2021). NDVI values range from -1 to 1 and indicate vegetation health and density.

2.8 El Niño Southern Oscillation

In order to account for the interannual variability of large-scale conditions the Niño 1+2 index was used to characterize the dominant Eastern equatorial Pacific sea surface temperature (SST) NOAA Climate Prediction Center (2024). They are closely linked to coastal and regional climate anomalies along the west coast of South America. It is particularly sensitive to the development of Eastern Pacific El Niño events, with positive values representing warm phases (El Niño) and negative values indicating cold phases (La Niña) Dubury and Duxbury (1999).

2.9 Data analysis

To identify the key environmental factors influencing the variability of GPP and Reco, we applied a Principal Component Analysis (PCA) using the scikit-learn Python package sci (2026). PCA is a statistical approach that reduces the dimensionality of the dataset by transforming correlated variables into a smaller set of uncorrelated variables, i.e. principal components, which capture the maximum variance in the data Jolliffe (2011). The primary objective of PCA was to identify dominant modes of

https://doi.org/10.5194/egusphere-2026-222
Preprint. Discussion started: 22 January 2026

covariability and to clarify which environmental variables exert the strongest control on GPP and Reco. In this study, PCA was applied to a set of meteorological, energy and carbon flux variables. The analysis was conducted on daily data for the defined seasons and on annual subsets mentioned above.

3 Results

3.1 Micrometeorological conditions

The study area exhibits distinct wet and dry seasons driven by high variability in precipitation and further climatic factors. As shown in Fig. 2, the wet season typically spans from January to May, and February 2025 in particular recorded the highest monthly precipitation at 302 mm. During the three-year period, the average total precipitation during the wet season was approximately 359 mm. The dry season extends from June to December, and is characterized by significantly lower rainfall averaging 6.8 mm, though 2023 was an exception with 41.8 mm. Correspondingly, SM reaches its peak during the wet period with a shift in the maximum from April 2023 (40 %vol.) to February 2025 (40%vol.), while it drops to 15%vol. during the dry months.

This is also reflected in the water balance derived from precipitation and ET (Fig. 2 d). Wet periods typically yield a positive water balance, except January 2024, which was almost neutral at 1.1 mm. In contrast, the dry period consistently shows a negative water balance (-11 mm). December, which marks the transition from dry to wet season, has a positive water balance of 60 mm, except in 2022 and 2024 when neutral conditions prevail and with maximum positive water balance in Feb 2025 with highest rainfall.

The maximum and minimum Ta range between 28 - 30°C and 14 - 18 °C, respectively, exhibiting lower variability with minor fluctuations during dry and wet periods. In contrast, the vapor pressure deficit (VPD) shows higher variability corresponding to variations in precipitation with maximum values of up to 13 hPa during the dry season and minimum values during the wet period (3.4 hPa). The same pattern can be observed in Rg and Ts resembling strong seasonality at the study site. Interestingly, the peak phase in Ts during the dry period in 2023 reveals lower values (27 °C) compared to 2022 (30 °C) and 2024 (30 °C).

NDVI as an indicator of the greenness of the vegetation and the Niño 1+2 index are illustrated to underpin the intra- and interannual variability of the region. NDVI exhibits a clear seasonal pattern, with higher (lower) values during the wet (dry) season. The maximum of 0.74 occurred in March 2024, while the minimum of 0.22 was observed in November 2022 when vegetation activity was lowest. The Niño 1+2 index reveals strong interannual variability, with La Niña conditions (negative values) dominating until late 2022, followed by a pronounced El Niño phase (positive values) from April 2023 to early 2024. Neutral conditions recurred from April to October 2024, followed by a return to positive values starting in January 2025.

https://doi.org/10.5194/egusphere-2026-222
Preprint. Discussion started: 22 January 2026

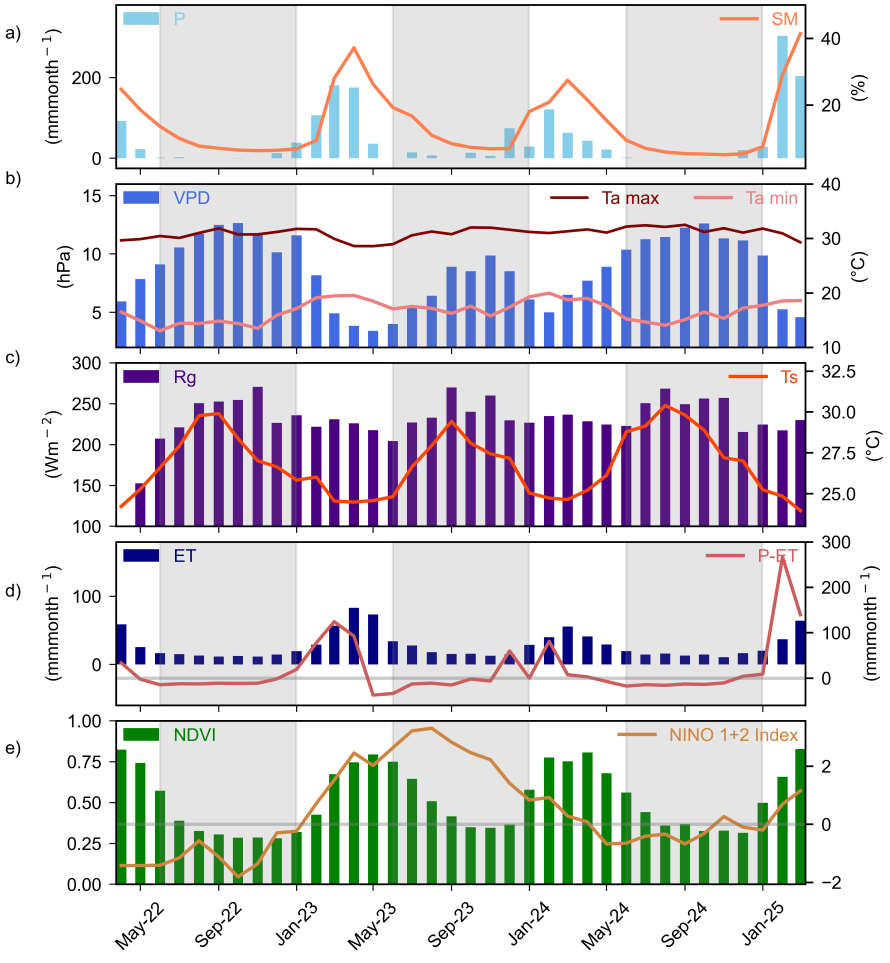

Figure 2. Monthly mean values of a) precipitation (P, bars, mm month^{-1}) and soil moisture (SM, line, %vol.), b) vapor pressure deficit (VPD, bars, hPa), maximum air temperature (Ta max, red line, °C), and minimum air temperature (Ta min, light red line, °C), c) global radiation (Rg, bars, W m^{-2}) and soil temperature (Ts, line, °C), (d) Evapotranspiration (ET, bars, mm month^{-1}) and Water balance calculated as Precipitation minus Evapotranspiration (P-ET, line, mm month^{-1}) and (e) Normalized difference vegetative index (NDVI, bars) and Nino 1+2 index (Nino 1+2 index, line) over the time period April 2022 to March 2025. The shaded area denotes the dry season. Note that Rg data for April 2022 is unavailable due to an instrument failure.

3.2 Energy Balance Closure

To assess the performance of the EC measurement system with respect to the EBC, Table 1 presents the regression coefficients (slope, intercept) of the linear fit of net-radiation (Rn) minus G against the sum of sensible (H) and latent (LE) heat flux grouped into the entire period, as well as wet, dry, and transition periods defined above in shown in FigA1.

https://doi.org/10.5194/egusphere-2026-222
Preprint. Discussion started: 22 January 2026

Data Periods	Intercept	Slope	R^2	RMSE
All Data	18.31	0.71	0.92	47.52
Wet	11.68	0.74	0.88	58.28
Dry	23.40	0.70	0.92	41.15
Transition (Wet -Dry)	21.13	0.71	0.88	35.44
Transition (Dry - Wet)	15.16	0.70	0.92	48.80

Table 1. Energy balance closure (EBC) metrics for various seasonal periods, including slope, intercept, R^2, and RMSE W m^{-2} values.

	Dry (2022)	Wet (2023)	Dry (2023)	Wet (2024)
Max	0.57	8.38	0.94	9.58
Min	0.15	4.00	0.15	2.22

Table 2. Soil CO_2 fluc (μmolm^{-2}s^{-1}) measured across the study area during survey campaigns carried out in the time periods listed.

In general, the EBC shows a strong correlation, accounting for 92% of the available energy (R^2 = 0.92). The slope of 0.71 indicates a moderate underestimation of turbulent energy fluxes, while the RMSE of 41.12 W m^{-2} indicates a reasonable level of error in all values. Closure is highest during the wet season, when the slope is 0.74. At the same time, the lowest R^2 value (0.88) is featured, which points to a greater variability in the data. This is further supported by the highest RMSE of 58.28 W m^{-2}. Closure is at its lowest (R^2 = 0.70) during the dry season and the transition to the wet season, while the transition to the dry season shows the lowest RMSE (35.44 W m^{-2}) suggesting reduced variability and more consistent measurements.

3.3 Seasonal patterns of carbon fluxes

Fig.3 presents the daily carbon fluxes throughout the study period, illustrating the dominant seasonal variations at our study site. Measurements begin in the wet season in April 2022, where we observe maximum values of NEP (-2.5 gC $m^{-2}day^{-1}$), GPP (7.5 gC m^{-2} day^{-1}), and Reco (5.0 gC m^{-2} day^{-1}). During the dry season, the magnitude of NEP decreases, fluctuating between -1 to -0.5 $gCm^{-2}day^{-1}$ from June to December (dry season), while GPP and Reco decrease to approximately half of their values compared to the wet season.

With respect to the carbon sink function, we can observe that the wet season is a strong carbon sequester with 11.2 $gCm^{-2}day^{-1}$ on average. This reduces to 2 $gCm^{-2}day^{-1}$ during the dry period.

This is also confirmed by the soil CO_2 flux summarized in table 2. Strong seasonal variations could be observed between the dry and wet season (measurements only available) with an increase in the efflux by 84% during the wet season.

Additionally, Table 3 summarizes the monthly carbon fluxes revealing the oscillation of carbon sink and source, particularly during the transitions. The wet season consistently acts as a carbon sink, especially in March, April, and May, when higher

https://doi.org/10.5194/egusphere-2026-222
Preprint. Discussion started: 22 January 2026

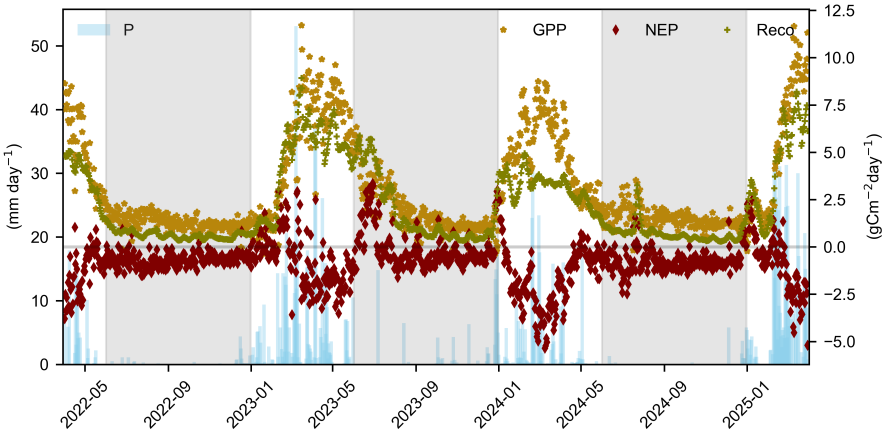

Figure 3. Daily sums of net ecosystem productivity (NEP, maroon marker, $gCm^{-2}day^{-1}$), gross primary productivity (GPP, yellow marker, $gCm^{-2}day^{-1}$) and ecosystem respiration (Reco, green marker, $gCm^{-2}day^{-1}$) throughout the study period. The shaded area indicates the dry season and daily precipitation (P, blue bar, mm day^{-1}).

rainfalls occur. The transition from wet to dry (June and July 2023) indicates a carbon source, while the dry-wet transition in January, February, and December 2023 features neutral carbon balances.

3.4 Annual carbon budgets and environmental factors

In order to examine variations between the three-year period, the annual distributions of GPP, Reco, and key environmental factors are summarized in Fig. 4. GPP and Reco exhibit the highest median and variability in 2023–2024, showing higher photosynthetic activity. Ts consistently exceed Ta across all years, with both remaining relatively stable for 2022-2023 and 2023-2024, but a slight increase is obtained in 2024-2025. SM and precipitation also have the highest values in 2023–2024, corroborating with lower VPD levels, and higher GPP and NDVI values.

In contrast, 2024–2025 shows reduced precipitation and SM, likely contributing to lower GPP and NDVI, while VPD levels are high representing increased atmospheric dryness.

Cumulative GPP, Reco, and NEP fluxes as well as precipitation are shown in Fig. 5 to summarize the annual and seasonal carbon budget. The markers indicate the onset of the respective seasons. The annual GPP and Reco sums highlight distinct differences between the three years. In 2023–2024, carbon fluxes were markedly elevated, with carbon uptake reaching 1377.9 $gCm^{-2}year^{-1}$ and carbon release at 1041.5 $gCm^{-2}year^{-1}$. In contrast, the remaining years (2022-2023 and 2024-2025) show similar patterns and reach GPP values of 939.6 and 977.2 $gCm^{-2}year^{-1}$ as well as Reco values of 710.19 and 685.64 $gCm^{-2}year^{-1}$. Interestingly, the onset of the respective seasons starts later in 2022-2023. This is also reflected in NEP with the highest carbon exchange of -336.36 $gCm^{-2}year^{-1}$, although variations in the wet-to-dry and dry-to-wet transitions can be observed. In particular, in 2023-2024 the wet-to-dry season shows a shift of the NEP values from negative to positive, which indicates a stronger carbon release into the atmosphere. The ecosystem functions as a carbon source during the dry

https://doi.org/10.5194/egusphere-2026-222
Preprint. Discussion started: 22 January 2026

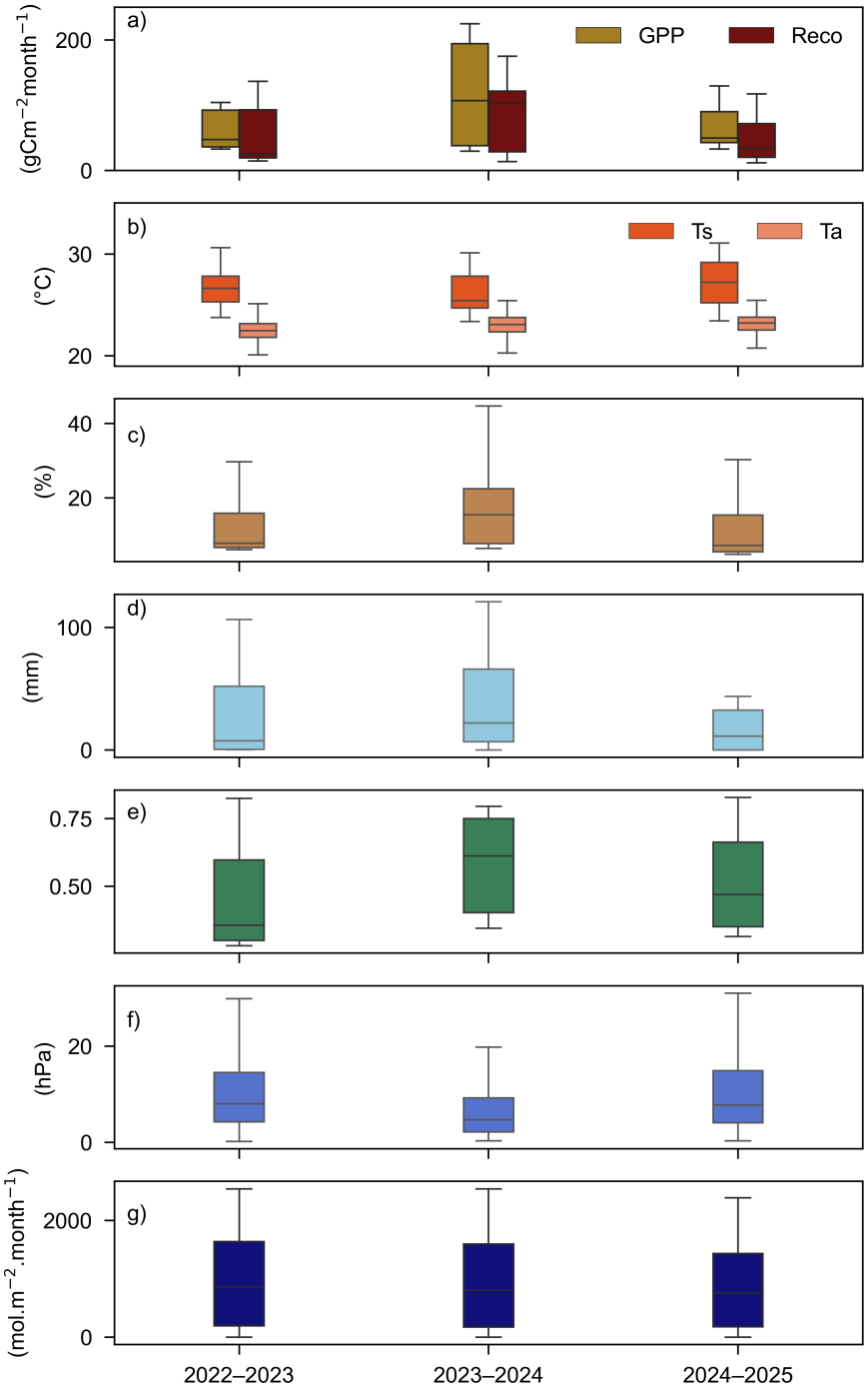

Figure 4. Yearly box plots of a) gross primary production (GPP, gCm^{-2} month^{-1}) and ecosystem respiration (Reco, gCm^{-2} month^{-1}), b) soil temperature (Ts, °C) and air temperature (Ta, °C), c) soil moisture (SM, % vol.), d) precipitation (P, mm month^{-1}), e) normalized difference vegetation index (NDVI) and f) vapor pressure deficit (VPD, hPa) for the years 2022–2023, 2023–2024 and 2024-2025.

https://doi.org/10.5194/egusphere-2026-222
Preprint. Discussion started: 22 January 2026

Year	Month	NEP	GPP	Reco	VPD	Ts	SM
2022	Apr	-63.9	195.2	131.3	5.9 ± 4.1	24.2 ± 0.7	24.7 ± 2.3
	May	-16.8	104.5	87.7	7.8 ± 5.6	25.2 ± 1.2	18.5 ± 1.7
	Jun	-18.77	47.62	28.85	9.1 ± 5.7	26.6 ± 1.2	13.5 ± 1.4
	Jul	-25.70	47.76	22.06	10.6 ± 6.4	27.9 ± 1.7	10 ± 0.7
	Aug	-26.17	47.76	21.75	11.7 ± 7.2	29.8 ± 1.9	7.7 ± 0.3
	Sep	-21.15	35.67	14.42	12.5 ± 7.0	29.9 ± 1.9	7.0 ± 0.2
	Oct	-19.06	35.30	16.24	12.6 ± 7.0	28.4 ± 1.5	6.5 ± 0.1
	Nov	-18.77	33.00	14.23	11.8 ± 7.2	27 ± 1.2	6.3 ± 0.1
	Dec	-13.54	33.73	20.18	10.1 ± 6.2	27 ± 0.9	6.4 ± 0.2
2023	Jan	-1.0	37.7	36.6	11.6 ±7.0	25.8 ± 1.2	6.9 ± 0.4
	Feb	17.7	87.4	105.2	8.2 ± 6.6	26 ± 1.3	9.4 ± 3.2
	Mar	-23.0	225.6	202.6	4.9 ± 4.2	24.5 ± 0.7	28 ± 9.5
	Apr	-49.1	222.5	173.3	3.8± 3.2	24.5± 0.9	37.1 ± 8.2
	May	-54.8	221.4	166.6	3.4 ± 2.7	24.6 ± 0.9	26.2 ± 4.9
	Jun	35.0	115.6	150.6	4.0 ± 3.2	24.8 ± 1.3	19.2± 2.2
	Jul	6.1	96.8	102.9	5.6± 4.6	26.6± 2.0	16.7± 1.7
	Aug	-22.6	58.4	35.8	6.4± 5.1	27.9± 2.3	10.9± 0.6
	Sep	-18.70	40.40	21.7	8.9± 5.8	29.4± 2.3	8.4± 0.6
	Oct	-9.08	30.76	21.6	8.5± 6.2	28± 2.0	7.3± 0.2
	Nov	-16.57	30.03	13.45	9.9± 6.5	27.4± 2.2	6.8± 0.2
	Dec	1.4	30.2	31.7	8.5± 6.3	27.1± 2.0	6.9± 1.2
2024	Jan	-19.3	124.3	105.0	6.1± 4.5	25.0± 0.9	17.5± 3.4
	Feb	-75.35	184.93	109.5	5.0± 4.1	24.7± 0.7	20.8± 9.2
	Mar	-104.35	209.09	104.7	6.5± 4.5	24.6± 0.7	27.3± 9.2
	Apr	-40.55	129.79	89.2	7.7± 5.3	25.2± 1.2	21.5± 6.5
	May	-12.9	78.9	66.0	8.9± 5.7	26.1± 1.5	15.3± 1.9
	June	-22.60	51.29	28.6	10.3± 6.4	28.7± 2.1	9.4± 1.1
	July	-25.04	63.63	38.59	11.2± 7.6	29.0± 2.2	7.0± 0.5
	Aug	-20.68	43.68	23.02	11.4± 7.5	30.3± 2.7	5.9± 0.3
	Sep	-28.74	45.26	16.51	12.2± 7.5	29.7± 2.4	5.4± 0.2
	Oct	-25.65	39.92	14.27	12.6± 7.2	28.8± 2.8	5.2± 0.1
	Nov	-25.30	36.79	11.49	11.3± 7.8	27.1± 2.0	5.0± 0.1
	Dec	-11.46	32.62	21.16	11.1± 6.6	27.0± 2.0	5.3± 0.1
2025	Jan	10.3	48.3	58.6	9.8 ± 6.6	25.2± 1.9	7.5± 0.7
	Feb	-5.7	123.1	117.3	5.2± 5.2	24.8± 1.3	29.0± 16.2
	Mar	-83.4	284.6	201.2	4.5± 3.7	23.9± 0.7	41.4± 3.3

Table 3. Monthly values of net ecosystem productivity (NEP, $gCm^{-2}month^{-1}$), gross primary productivity (GPP, $gCm^{-2}month^{-1}$) and ecosystem respiration (Reco, $gCm^{-2}month^{-1}$), vapor pressure deficit (VPD, hpa), soil temperature (Ts, °C) and soil moisture (SM, %vol.) in values for years 2022, 2023, and 2024

season and temporarily in January to February. During 2022-2023 and 2024-2025, a more consistent annual pattern sink is shown with maximum values of –229.49 and –291.58 $gCm^{-2}year^{-1}$, respectively.

290 To quantify the relationship between the carbon fluxes and environmental conditions Fig. 6 displays annual GPP and Reco values against key environmental factors such as VPD, Ts, SM and NDVI. Ta and RH are not shown as it shows no further insights into the relationship. Standard deviations of each variable calculated on a monthly basis show the strength of the variability.

https://doi.org/10.5194/egusphere-2026-222
Preprint. Discussion started: 22 January 2026

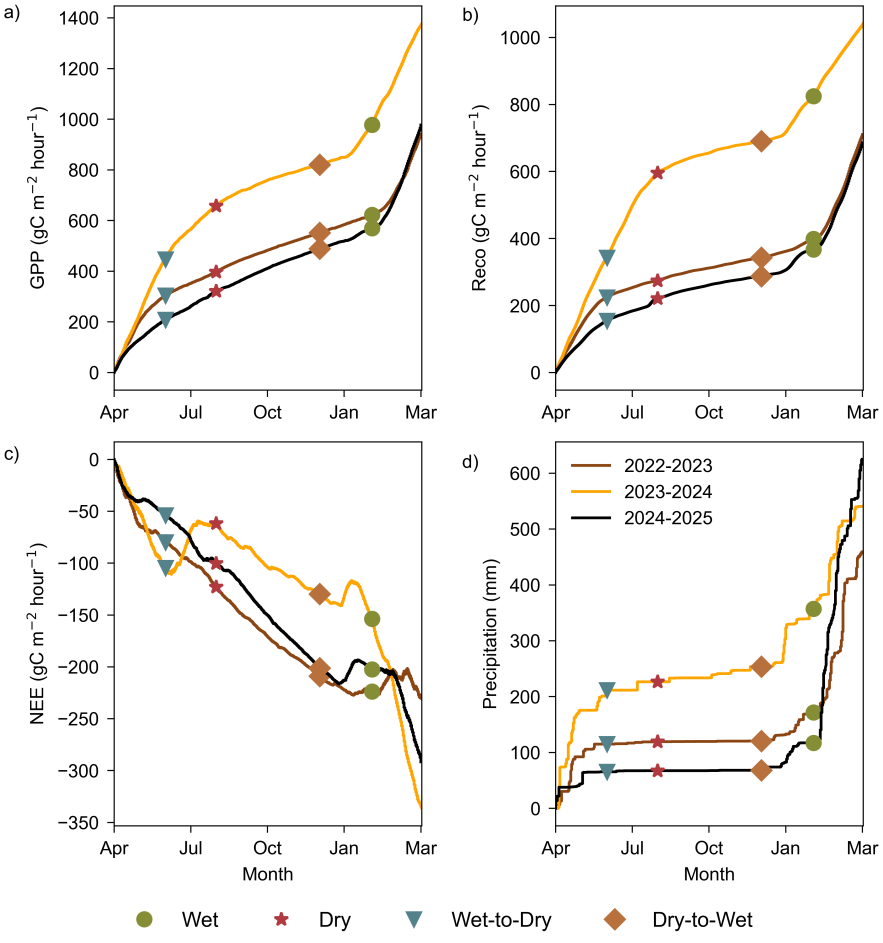

Figure 5. Cumulative distribution of a) gross primary productivity (GPP, gCm^{-2}hour^{-1}), b) ecosystem respiration (Reco, gCm^{-2}hour^{-1}), c) net ecosystem productivity (NEP, gCm^{-2}hour^{-1}), and d) precipitation (P, mm). Markers indicate the onset of the defined seasonal phases wet (dot,green), dry (star, red), wet-to-dry (triangle. blue), and dry-to-wet (diamond, orange). Data are shown for the years 2022-2023 (line, brown), 2023-2024 (line,orange), and 2024-2025 (line, black).Note that measurements begin in April.

https://doi.org/10.5194/egusphere-2026-222
Preprint. Discussion started: 22 January 2026

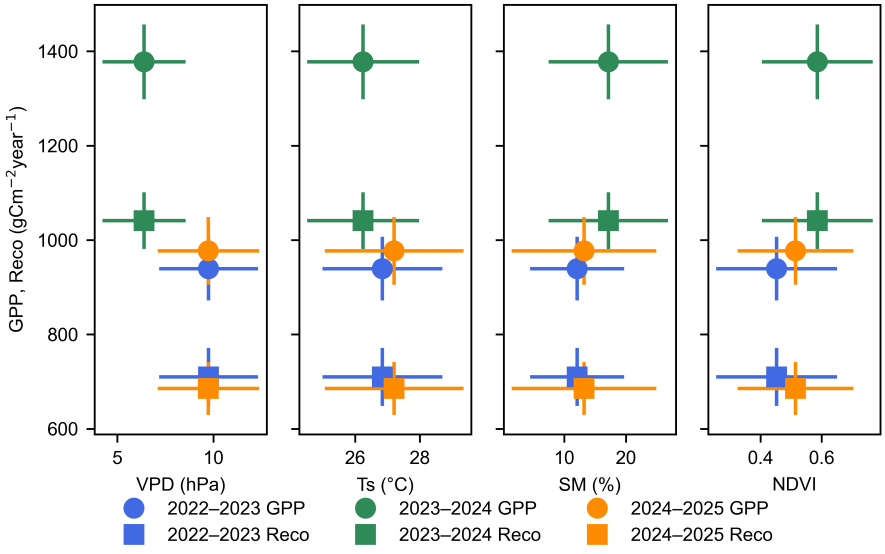

Figure 6. Annual relationships between gross primary production (GPP) and ecosystem respiration (Reco) with key environmental drivers vapor pressure deficit (VPD, hPa), soil temperature (Ts, °C), soil moisture (SM, % vol.), and normalized difference vegetation index (NDVI) across three annual periods 2022–2023 (blue), 2023–2024 (green), and 2024–2025 (orange). Circle markers represent GPP and square markers represent Reco for each respective year.

Annual carbon fluxes in 2022–2023 (GPP: 939, Reco: 710) and 2024–2025 (GPP:977, Reco: 685) show similar patterns, with clearly lower levels compared to 2023–2024 (GPP: 1377, Reco: 1041). At the same time, VPD and Ts reveal lower values in 2023-2024 reaching only 10hPa and 27°C on average, while SM and NDVI show higher values up to 0.6, reflecting favorable growing conditions.

3.5 Seasonal and annual functional relationships

To examine how seasonal availability of water and light impacts the carbon fluxes of the dry forest ecosystem. Fig. 7 illustrates WUE and LUE grouped by the defined seasons and years. WUE appears relatively consistent across all seasons with median values varying between 3 and 5 gC kg^{-1}H$_2$O. Differences between the years are more pronounced. While 2022-2023 and 2024-2025 show similar patterns across the seasons, 2023-2024 had higher values during the wet and dry-to-wet period. In the remaining seasons this year showed lower values. Therefore, fluctuations in WUE are more evident on the inter- than intrannual basis.

In contrast, LUE shows a more pronounced seasonality with the highest values on average during the wet season (4.8 gC MJ^{-1}) and a clear decline towards the dry season (1.5 gC MJ^{-1}). The highest LUE occurs in the wet season in 2023-2024, but also the dry-to-wet season during this year exhibits strikingly high values compared to the remaining two years (2.5 gC MJ^{-1}).

https://doi.org/10.5194/egusphere-2026-222
Preprint. Discussion started: 22 January 2026

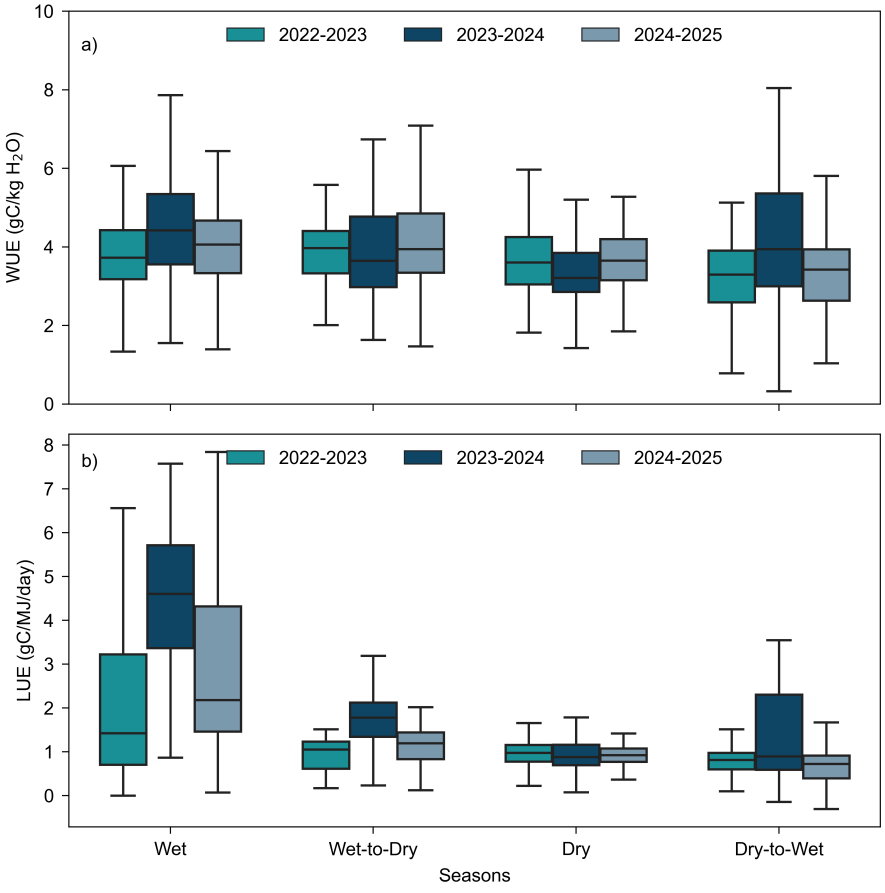

Figure 7. Box plots representing a) water use efficiency (WUE, gC $kg^{-1}H_2O$) and b) light use efficiency (gC MJ^{-1}) across different seasonal periods (wet, dry, wet-to-dry transition, and dry-to-wet transition) over three annual periods 2022–2023, 2023–2024, and 2024–2025.

Cumulative distributions of WUE and LUE are illustrated in Fig. 8. Similarly to seasonal patterns, WUE also shows a rather weak signal in the interannual variability and rises almost linearly throughout each year, but 2023-2024 has higher when compared with other time periods.

In contrast, LUE reveals clear differences between the years. 2023–2024 presents a markedly higher cumulative LUE, particularly due to stronger increases from June, indicating enhanced light utilization and productivity. This features a different growth pattern compared to the other two years, which differ mainly by magnitude with 2022-2023 showing the lowest LUE values.

https://doi.org/10.5194/egusphere-2026-222
Preprint. Discussion started: 22 January 2026

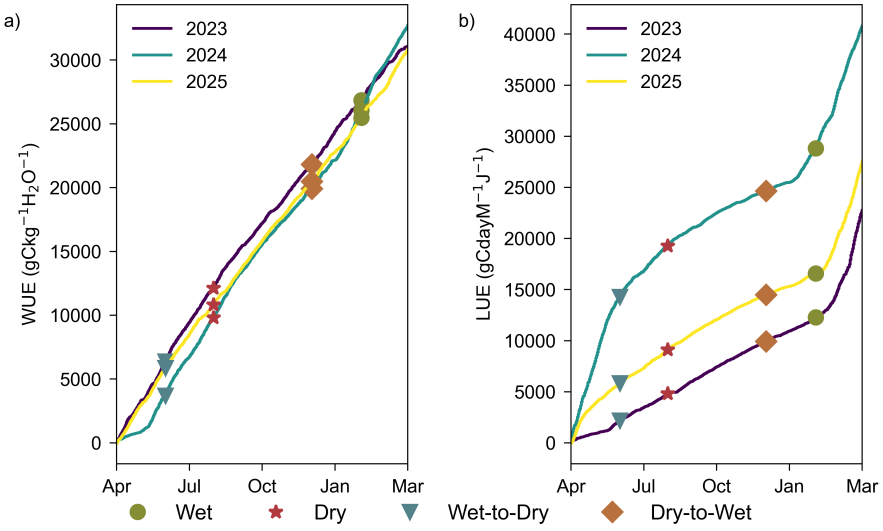

Figure 8. Cumulative distribution of a) water use efficiency (WUE, gCkg^{-1}H2O) and b) light use efficiency (gC MJ^{-1}). MMarkers indicate the onset of the defined seasonal phases wet (dot,green), dry (star, red), wet-to-dry (triangle. blue), and dry-to-wet (diamond, orange). Data are shown for the years 2022-2023 (line, purple), 2023-2024 (line,blue), and 2024-2025 (line, yellow). Note that measurements begin in April.

3.6 Environmental controls on carbon fluxes

While efficiency metrics provide direct indications of limitations imposed by water and light, multivariate analysis such as PCA allows the most important environmental controls to be systematically identified. Fig.9 illustrates bi-plots of environmental factors together with GPP and Reco classified into the four defined seasons loadings and variances mentioned in . For both carbon fluxes, the first two PCs explain most of the total variance. During the wet season PC1 shows strong positive loadings for Rg (0.92), Ta (0.85), VPD (0.81), H (0.85), LE (0.80), and GPP (0.80). This component therefore represents an energy or radiation driven gradient, where increased incoming radiation and temperature coincide with enhanced turbulent energy exchange and photosynthetic activity.

PC2 was characterized by high positive loadings for Ts (0.81) and VPD (0.45), and strong negative loadings for SM (–0.74), LE (–0.46), and GPP (–0.43). This axis thus captures a moisture-related gradient, separating wet, energy-efficient conditions from dry, water-limited conditions with reduced carbon uptake. In contrast, the PCA for Reco reveals a different structure. PC1 is dominated by positive loadings of Ta (0.89), VPD (0.87), Rg (0.88), and H (0.84), but Reco contributed little to this axis (0.05). It shows that respiration is not directly coupled to short-term variability in atmospheric energy availability. Instead, PC2 was characterized by high positive loadings of Reco (0.81), SM (0.82), and LE (0.51), and negative loadings of Ts (–0.68) and VPD (–0.28), suggesting that respiration rates are primarily controlled by moisture availability. During the dry season GPP (0.80) is again represented by PC1, reflecting the co-variation of photosynthetic activity with incoming radiation and turbulent

https://doi.org/10.5194/egusphere-2026-222
Preprint. Discussion started: 22 January 2026

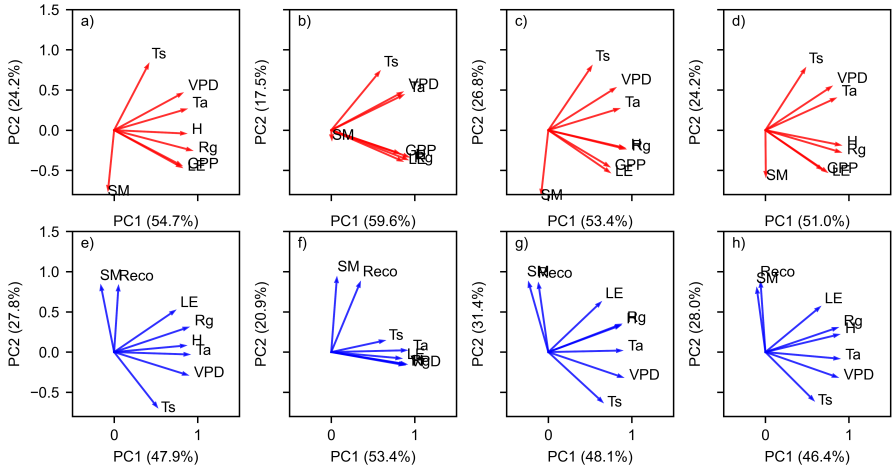

Figure 9. Principal Component Analysis (PCA) of gross primary production (GPP, red) and ecosystem respiration (Reco, blue) in relation to key environmental variables: soil temperature (Ts, °C), air temperature (Ta, °C), vapor pressure deficit (VPD, hPa), soil moisture (SM, % vol.), latent heat flux (LE, W m^{-2}), sensible heat flux (H, W m^{-2}), and global radiation (Rg, W m^{-2}) for the four seasonal conditions: (a,d) wet, (b,e) dry, (c,f) wet-to-dry transition, and (d,h) dry-to-wet transition.

heat exchange, but also weak negative loadings on PC2 (-0.29) together with LE (–0.38). This suggests that PC2 distinguishes hot and dry conditions from periods of higher evaporative and carbon uptake activity. Reco is strongly loading on PC2 (0.86), while SM contributed little to either component, indicating limited short-term influence of water on observed flux variability during the dry period. The transition season wet-to-dry shows a similar pattern to the wet season with a strong loading of GPP (0.72) on PC1 representing an energy-driven gradient, and negative loading of GPP (-0.45) on PC2. Reco again has a strong loading (0.84) on PC2 together with SM (0.86) and LE (0.61) as well as negative loadings of VPD (-0.31) reflecting the moisture related component. Dry-to-wet transition GPP (0.61) as well strongly loads onto PC1 and is driven by an energy- and radiation gradient. Interestingly, PC2 contrasted variables related to moisture (SM = -0.56, LE = -0.51) and temperature (Ts = 0.76, VPD = 0.54) with a negative loading of GPP (-0.48). Therefore, this component captures a moisture–dryness gradient, separating dry, hot periods with reduced GPP from wetter conditions with higher LE and carbon uptake. Reco is strongly loading onto PC2 (0.86), together with SM (0.78), and LE (0.55), and negative loadings for Ts (–0.59) and VPD (–0.31) indicating that respiration rates were primarily controlled by soil moisture availability.

To quantify the temporal stability of environmental controls and their contribution to the annual variability of carbon fluxes Fig. 10 shows the bi-plots for the years 2022-2023, 2023-2024 and 2024-2025. For the year 2022–2023, the PCA for GPP revealed that PC1 was dominated by positive loadings of Ta (0.84), VPD (0.83), H (0.87), Rg (0.89), and GPP (0.60), indicating that carbon uptake increased with higher radiation and associated energy fluxes. In contrast, PC2 showed strong negative loadings for GPP (–0.61) and LE (–0.64), and a high positive loading for Ts (0.76), suggesting that this component represents a temperature–moisture gradient, where GPP decreases under higher surface temperature conditions. For Reco, the PCA revealed

https://doi.org/10.5194/egusphere-2026-222
Preprint. Discussion started: 22 January 2026

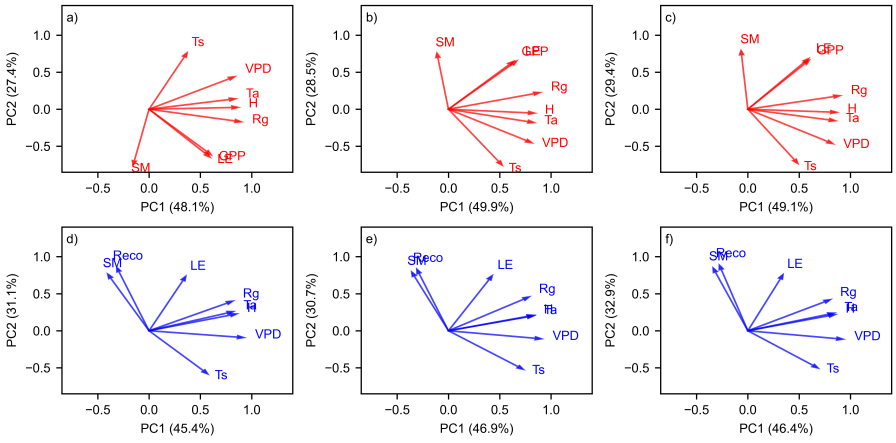

Figure 10. Principle Component Analysis PCA gross primary production (GPP, red) and ecosystem respiration (Reco, blue) in relation to key environmental variables soil temperature (Ts, °C), air temperature (Ta, °C), vapor pressure deficit (VPD, hPa), soil moisture (SM, % vol.), latent heat flux (LE, W m^{-2}), sensible heat flux (H, W m^{-2}) and global radiation (Rg, W m^{-2}) (a,d) 2022-2023 , (b,e) 2023-2024 and (c,f) 2024-2025

a different structure. PC1 was characterized by negative loadings for Reco (–0.32) and positive loadings for Ta (0.82), VPD (0.92), and H (0.85), indicating that respiration was weakly coupled to short-term variability in atmospheric energy. PC2 showed strong positive loadings for Reco (0.86) and LE (0.74), as well as a negative loading for Ts (–0.58) and a positive loading for SM (0.77), reflecting the influence of moisture availability on respiration rates.

In 2023–2024, the PCA for GPP showed that PC1 was again dominated by energy-related variables, with strong positive loadings for Ta (0.83), VPD (0.81), H (0.83), Rg (0.89), and GPP (0.63). This component represents an energy-driven gradient, where GPP increases with higher radiation and sensible heat flux. PC2 showed positive loadings for GPP (0.64) and LE (0.65), and a strong negative loading for Ts (–0.75) which is positive in 2022-2023, indicating that carbon uptake is enhanced under cooler and wetter conditions with higher latent heat flux. For Reco, PC1 was dominated by Ta (0.83), VPD (0.91), H (0.83), and Rg (0.79) with weak negative loading of Reco (–0.31), suggesting a limited direct link between respiration and short-term energy inputs. PC2 exhibited strong positive loadings of Reco (0.83), LE (0.75), and SM (0.79), together with a negative loading of Ts (–0.52), highlighting the key role of moisture availability in controlling respiration dynamics during this year.

For 2024–2025, the GPP PCA indicated that PC1 continued to reflect an energy-driven gradient with strong positive loadings of Ta (0.85), VPD (0.83), H (0.86), Rg (0.89), and GPP (0.59). This confirms that photosynthetic carbon uptake was primarily associated with radiation and energy fluxes. PC2 showed positive loadings for GPP (0.66), LE (0.68), and SM (0.79), and a strong negative loading for Ts (–0.73), representing a moisture–temperature gradient where GPP decreases under hot and dry conditions. For Reco, PC1 exhibited positive loadings for Ta (0.84), VPD (0.93), H (0.85), and Rg (0.80) with a weak negative loading for Reco (–0.28), suggesting that respiration was less influenced by instantaneous energy inputs. PC2 displayed

https://doi.org/10.5194/egusphere-2026-222
Preprint. Discussion started: 22 January 2026

strong positive loadings for Reco (0.89), LE (0.76), and SM (0.85), accompanied by a negative loading for Ts (–0.50), again emphasizing that respiration was primarily controlled by soil moisture and water fluxes.

4 Discussion

This study focuses on carbon balances in a Tumbesian dry forest ecosystem in southern Ecuador, characterized by strong seasonality and pronounced dry–wet transitions that critically influence ecosystem function. Intra- and interannual variability of carbon fluxes and environmental conditions was investigated using EC measurements installed above the forest canopy. The EBC as a critical measure in estimating the quality of the measured fluxes showed good slope values across the defined seasons, confirming the reliability of the data. They are in the range of 70 - 77% which can occur in more complex terrain and can reach up to 35% Cuxart et al. (2016).

Seasonality in the study region is particularly driven by atmospheric circulation patterns Garreaud (2000), which result in a rainy (dry) season when the ITCZ is located on the northern (southern) hemisphere and eastern (north-eastern) trade winds allowing (inhibiting) convective activities at the western slopes of the Andes Bendix et al. (2017). Thus, these large-scale patterns directly affect the timing and magnitude of local-scale rainfall distributions. Meteorological conditions at the study site reflected the strong seasonality, particularly in water-related variables such as precipitation, SM, RH and VPD (Fig. 2. Due to geographical location of the study site, Ta showed minimal seasonal variation, while Ts revealed distinct seasonal changes. The diverging Ta and Ts patterns indicates the differential thermal responses of the atmosphere and the land surface, with Ts being more responsive to changes in Rg, SM availability, and surface energy partitioning. ET, intrinsically coupled to both water availability and temperature, exhibits seasonal dynamics reflecting the combined influence of these environmental drivers also observed in Nie et al. (2021).

Seasonal variations in carbon exchange were evident throughout the study period (April 2022 – March 2025). Peak carbon uptake occurred between February and May (600-725 $gCm^{-2}year^{-1}$), coinciding with the rainy season. This interval represents the main growth period, characterized by high photosynthetic activity due to the concurrent availability of water and light, as reflected by elevated NDVI values (Fig. 2). During this phase, the dry forest acted as a strong carbon sink (NEP ranging from -100 to -200 $gCm^{-2}year^{-1}$) comparable to neotropical dry forests in Mexico Rojas-Robles et al. (2020). Quantified GPP values were proportional to the magnitude of precipitation (Table 3) highlighting the importance of water availability, consistent with findings from dry forest ecosystems in Costa Rica Castro et al. (2018) and southern California Luo et al. (2007).

Despite declining photosynthetic activity and leaf fall due to reduced atmospheric moisture during the wet-to-dry transition, the area still acted primarily as a carbon sink. However, rainfall anomalies in June-July 2023 (10.5 mm compared to 3.5 mm) caused NEP to indicate a carbon source (35.6 $gCm^{-2}month^{-1}$), likely due to the Birch effect triggering increased soil microbial respiration Jarvis et al. (2007); González-Jaramillo et al. (2016). This caused Reco to exceed GPP, also described by Rojas-Robles et al. (2020), with the forest temporarily functioning as a carbon source (Tab. 3).

During the dry-to-wet transition, the ecosystem demonstrated carbon flux responses ranging from near-neutral to net CO_2 source behavior, depending strongly on the timing and intensity of early-season precipitation. For instance, early rainfall

https://doi.org/10.5194/egusphere-2026-222
Preprint. Discussion started: 22 January 2026

during the 2022-2023 wet season caused the ecosystem to act as a net carbon source in February 2023, with NEP values of +17 $gCm^{-2}month^{-1}$ (Table 3). In contrast, during the dry season, limited water availability reduced photosynthetic activity, decreasing carbon accumulation by approximately 85% compared to the wet season. This decline was reflected in reduced NDVI values, consistent with observations from tropical dry forests in the Catinga biome in Brazil Mendes et al. (2020) and cool dry forests in Argentina García et al. (2017). Elevated VPD during the dry period further constrained carbon uptake by promoting stomatal closure and limiting gas exchange (Fig. 2). The dominant factor on seasonal carbon fluxes was the pronounced reduction in photosynthetically active area during the dry season, as deciduous and semi-deciduous species shed their leaves. Nevertheless, the ecosystem generally remained a net carbon sink, likely sustained by ongoing photosynthesis of evergreen species in the area.

At the annual scale, clear variations in ecosystem productivity were observed during the study period. Consistent with previous studies Mendes et al. (2020); González-Jaramillo et al. (2016); García et al. (2017) the tropical dry forests functioned as a net carbon sink, with annual budgets ranging from -100 to -300 $gCm^{-2}year^{-1}$. In our study area, annual carbon balances fell within this range (-200 to -250 $gCm^{-2}year^{-1}$; Tab. 3). Despite this overall sink behavior, strong interannual variability was evident. GPP peaked in 2023–2024 (1377 $gCm^{-2}year^{-1}$), while substantially lower values were observed in 2022–2023 (939 $gCm^{-2}year^{-1}$) and 2024–2025 (977 $gCm^{-2}year^{-1}$). The elevated productivity in 2023–2024 coincided with favorable hydroclimatic conditions, characterized by higher SM (37%) and reduced atmospheric water stress (VPD around 9 hpa) (Fig.3), which indicates enhanced water availability and canopy photosynthetic activity. In contrast, reduced productivity in the other years was associated with increased water stress. The moderate recovery observed in 2024–2025 is likely linked to improved post El Nino soil water storage, partially offsetting hydroclimatic constraints.

El Niño phases are typically linked to reduced ecosystem productivity, particularly in hydroclimatic sensitive tropical and semiarid regions Dannenberg et al. (2021) with the strongest impacts during Central Pacific El Niño events due to elevated temperatures and increased atmospheric water demand. Restrepo-Coupe et al. (2024) showed that El Niño-induced droughts in the tropical Amazon substantially reduced photosynthetic capacity through elevated VPD, decreased canopy conductance, and leaf area loss, with persistent legacy effects, while La Niña wet extremes primarily imposed light limitation and allowed for rapid recovery. In our study, the moderate productivity observed in 2024–2025 likely indicates improved post El Niño soil water storage, while reduced productivity in 2022–2023 and parts of 2024–2025 can be attributed to increased water stress and suppressed photosynthetic activity.

Linking efficiency metrics to EC-derived carbon fluxes revealed that seasonal and interannual variability in carbon exchange is predominantly controlled by light-use processes rather than water-use constraints. Both, WUE and LUE strongly depend on hydroclimatic transitions, but their dynamics differ systematically (Fig. 6). During the wet season, high efficiencies indicate favorable conditions for carbon uptake. As conditions shift towards the dry season, LUE declines earlier than WUE likely driven by early leaf shedding and reduced canopy light absorption. This highlights the sensitivity of light-use processes to phenological adjustments that precede severe water stress. Under dry-season conditions, both efficiencies converge at low values, showing physiological down-regulation of photosynthesis and reduced autotrophic respiration Zhang et al. (2015); Zeng et al. (2025). On the other hand, during the dry-to-wet transition the rapid recovery of LUE compared to WUE suggests that canopy

https://doi.org/10.5194/egusphere-2026-222
Preprint. Discussion started: 22 January 2026

greening (higher NDVI) and radiation-driven controls on photosynthesis precede the full restoration of ecosystem water use Nie et al. (2021).

At the interannual scale, cumulative LUE peaked in 2023–2024, was intermediate in 2024–2025, and lowest in 2022–2023, whereas WUE remained relatively stable throughout the study period (Fig. 8). The reduced efficiency in 2022–2023 is likely due to drier conditions that constrained both water availability and photosynthetic capacity. The strong correspondence between annual LUE and GPP indicates that light-use processes dominate interannual variability in carbon fluxes. This is consistent with findings from tropical FLUXNET sites, where year-to-year variations in GPP are primarily regulated by radiation-driven photosynthetic efficiency and canopy functioning, while WUE exhibits weaker interannual variability Zhang et al. (2015); Tan et al. (2015).

Our PCA results provide mechanistic insights into the environmental drivers shaping carbon flux dynamics in this tropical dry forest (Fig. 9; Table 3). Across seasons, Reco (strongest loading on PC2 between 0.81 - 0.86) was consistently controlled by SM, reflecting the fundamental moisture dependence of microbial decomposition consistent with patterns reported by Rodda et al. (2021); Rojas-Robles et al. (2020) for tropical forests, whereas temperature effects were secondary and modulated by water availability. During wet and transition periods, higher temperatures slightly reduced Reco (loading between -0.59 to -0.61), likely due to enhanced moisture constraints, whereas in the dry season, low SM dominated respiration, limiting the influence of temperature Cusack et al. (2023).

In contrast, GPP exhibited pronounced seasonal shifts in its dominant controls. During the wet season, photosynthesis was primarily energy-driven, responding to Rg, Ta, and turbulence, consistent with a non-limiting water regime. Under dry conditions and during transitional periods, GPP became increasingly sensitive to SM and VPD, revealing a strong moisture limitation and a temporary decoupling between photosynthesis and respiration. During the wet-to-dry transition, decreasing SM and increasing VPD constrained GPP despite sufficient energy, whereas Reco quickly responded to moisture pulses Stan and Sanchez-Azofeifa (2019). In contrast, during the dry-to-wet transition this decoupling between soil and atmospheric moisture implies a lagged recovery of carbon uptake Castro et al. (2018).

At the annual scale, contrasting sensitivities of GPP and Reco highlight an asymmetric ecosystem response to hydroclimatic variability (Fig. 10). Reco remained largely moisture-controlled across years, reflecting the robustness of decomposition processes to interannual climatic fluctuations Davidson and Janssens (2006). In contrast, GPP shifted between moisture- and energy-limited regimes depending on hydroclimatic conditions. In 2022–2023, moisture limitation dominated, while the El Niño–influenced 2023–2024 period (Niño 1+2 index between 2.4 – 3.4, Fig. 2) exhibited energy-controlled photosynthesis due to sustained high SM, a pattern that persisted into 2024–2025. Similar ENSO-driven shifts in carbon flux controls have been documented in Amazonian forests Restrepo-Coupe et al. (2024).

These findings are governed by a dynamic interplay between soil moisture and energy availability. While Reco is consistently constrained by water availability, GPP is highly responsive to both moisture and energy gradients, resulting in asymmetric re-

https://doi.org/10.5194/egusphere-2026-222
Preprint. Discussion started: 22 January 2026

sponses to drought and wet extremes. This decoupling has important implications: drought suppresses both photosynthesis and respiration, but short-term carbon gains can occur when respiration responds faster to moisture pulses Janssen et al. (2020); Restrepo-Coupe et al. (2024). Moreover, the persistence of altered GPP variability under extreme hydroclimatic events underscores the vulnerability of these forests to increasing drought frequency and intensity, with potential consequences for regional carbon cycling and climate feedbacks Castellanos et al. (2022).

5 Conclusions

This study analyzed seasonal and annual carbon fluxes of a tropical dry forest ecosystem in Southern Ecuador using EC measurements, which revealed a strong sensitivity of ecosystem carbon exchange to microclimatic variability. The quantified carbon balance showed that the ecosystem plays a dynamic role in the regional carbon cycle and is highly responsive to climatic variations. Although the forest acted as a net carbon sink over the study period, pronounced seasonal and interannual variability was observed, including temporary shifts to carbon source conditions during periods of climatic stress. The absence of pronounced seasonality in WUE indicated a clearly regulated and stable stomatal control of carbon–water exchange throughout the year. In contrast, LUE exhibited strong seasonal variability, reflecting pronounced phenological and biochemical controls on radiation use driven by seasonal changes in leaf area. Water availability further modulated the magnitude of carbon fluxes. Wetter years were characterized by enhanced GPP and Reco, associated with lower VPD, as well as higher SM and NDVI. Drier years showed reduced carbon uptake due to environmental constraints on ecosystem functioning. This interannual variability in carbon fluxes and microclimatic conditions was linked to large scale climate patterns including, particularly shifts in different phases of ENSO. Seasonal and annual controls on the carbon fluxes were confirmed by the PCA. Generally, GPP was driven by Rg and Ta while Reco was rather impacted by SM and Ts. At the annual scale, GPP in particular was influenced by varying environmental factors. ENSO-related climate extremes altered established relationships by shifting the balance between energy and moisture limitations. Periods of increased atmospheric dryness and elevated temperatures led to a partial decoupling of photosynthesis and respiration, with GPP showing high sensitivity to hydroclimatic stress, while Reco remained more consistently regulated by soil moisture availability. Overall, the results confirm that SM is a critical controlling factor in water-limited tropical dry forest ecosystems. However, they also demonstrate that ecosystem functioning emerges from interacting atmospheric and soil processes, whereby even small changes in Ts, Rg, and VPD can substantially alter ecosystem feedbacks. These findings provide valuable insights into the vulnerability of tropical dry forests to climate variability and their potential role in climate change adaptation and mitigation strategies.

https://doi.org/10.5194/egusphere-2026-222
Preprint. Discussion started: 22 January 2026

Table A1. Critical values used for filtering NEE, H and LE data. I_u and I_w represent turbulent indices.

Season	Filter	Day	Night
2022 Dry Season	I_u	4.2	2.5
	I_w	-0.05, 0.01	-0.05, 0.01
2022 Wet Season	I_u	2.0	1.6
	I_w	-0.10, 0.24	-0.13, 0.09
2022 Transition (wet-dry)	I_u	2.4	3.8
	I_w	-0.01, 0.23	-0.01, -0.04
2022 Transition (dry-wet)	I_u	2.3	3.6
	I_w	-0.17, 0.36	-0.14, 0.38
2023 (wet)	I_u	4.0	2.5
	I_w	-0.03, 0.35	-0.23, 0.00
2023 Transition (wet-dry)	I_u	1.9	3.3
	I_w	-0.05, 0.23	-0.27, 0.08
2023 (dry)	I_u	3	1.9
	I_w	-0.04, 0.32	-0.02, 0.07
2023 Transition (dry-wet)	I_u	3.6	2.3
	I_w	-0.11, 0.36	-0.43, 0.13
2024 (wet)	I_u	4.3	2.8
	I_w	-0.02, 0.2	-0.04, 0.14
2024 (wet-dry)	I_u	2.3	2.8
	I_w	-0.12, -0.03	-0.04, -0.14
2024 (dry)	I_u	4.1	2.8
	I_w	-0.02, -0.34	-0.01, 0.05
2024 (dry-wet)	I_u	2.3	2.8
	I_w	-0.02, 0.34	-0.04, -0.01
2025 (wet)	I_u	4.5	2.8
	I_w	-0.05, 0.01	-0.01, -0.05

https://doi.org/10.5194/egusphere-2026-222
Preprint. Discussion started: 22 January 2026

Table B1. PCA loadings (%) for GPP and Reco across all seasons.

Season	Variable	GPP PC1	GPP PC2	Reco PC1	Reco PC2
Wet	Target	0.80	-0.43	0.05	0.81
	Ta	0.85	0.26	0.89	-0.03
	VPD	0.81	0.45	0.87	-0.28
	H	0.85	-0.04	0.84	0.08
	LE	0.80	-0.46	0.72	0.51
	Rg	0.92	-0.25	0.88	0.30
	Ts	0.41	0.81	0.51	-0.68
	SM	-0.07	-0.74	-0.16	0.82
Dry	Target	0.80	-0.29	0.34	0.86
	Ta	0.85	0.43	0.89	0.02
	VPD	0.84	0.47	0.86	-0.16
	H	0.92	-0.33	0.89	-0.15
	LE	0.84	-0.38	0.82	-0.08
	Rg	0.90	-0.36	0.87	-0.15
	Ts	0.57	0.72	0.63	0.14
	SM	0.01	-0.11	0.07	0.92
Wet-Dry	Target	0.72	-0.45	-0.12	0.84
	Ta	0.83	0.26	0.87	0.02
	VPD	0.79	0.52	0.88	-0.31
	H	0.90	-0.22	0.85	0.33
	LE	0.73	-0.52	0.62	0.61
	Rg	0.91	-0.23	0.86	0.34
	Ts	0.51	0.79	0.64	-0.61
	SM	-0.08	-0.79	-0.23	0.86
Dry-Wet	Target	0.67	-0.48	-0.06	0.86
	Ta	0.83	0.39	0.87	-0.08
	VPD	0.78	0.54	0.85	-0.31
	H	0.89	-0.18	0.87	0.22
	LE	0.73	-0.51	0.65	0.55
	Rg	0.89	-0.27	0.85	0.30
	Ts	0.47	0.76	0.57	-0.59
	SM	0.01	-0.56	-0.10	0.78

https://doi.org/10.5194/egusphere-2026-222
Preprint. Discussion started: 22 January 2026

Table C1. GPP and Reco ladings(%) for given years.

Year	Variable	PC1 GPP	PC2 GPP	PC1 Reco	PC2 Reco
2022-2023	Target	0.60	-0.61	-0.32	0.86
	Ta	0.84	0.14	0.82	0.26
	VPD	0.83	0.43	0.92	-0.09
	H	0.87	0.02	0.85	0.23
	LE	0.59	-0.64	0.36	0.74
	Rg	0.89	-0.16	0.82	0.40
	Ts	0.37	0.76	0.57	-0.58
	SM	-0.15	-0.17	-0.40	0.77
2023-2024	Target	0.63	0.64	-0.31	0.83
	Ta	0.83	-0.17	0.83	0.20
	VPD	0.81	-0.45	0.91	-0.11
	H	0.83	-0.05	0.83	0.21
	LE	0.66	0.65	0.43	0.75
	Rg	0.89	0.22	0.79	0.46
	Ts	0.52	-0.75	0.73	-0.52
	SM	-0.11	0.75	-0.36	0.79
2024-2025	Target	0.59	0.66	-0.28	0.89
	Ta	0.85	-0.15	0.84	0.24
	VPD	0.83	-0.46	0.93	-0.11
	H	0.86	-0.04	0.85	0.22
	LE	0.59	0.68	0.34	0.76
	Rg	0.89	0.18	0.80	0.42
	Ts	0.48	-0.73	0.69	-0.50
	SM	-0.06	0.79	-0.34	0.85

https://doi.org/10.5194/egusphere-2026-222
Preprint. Discussion started: 22 January 2026

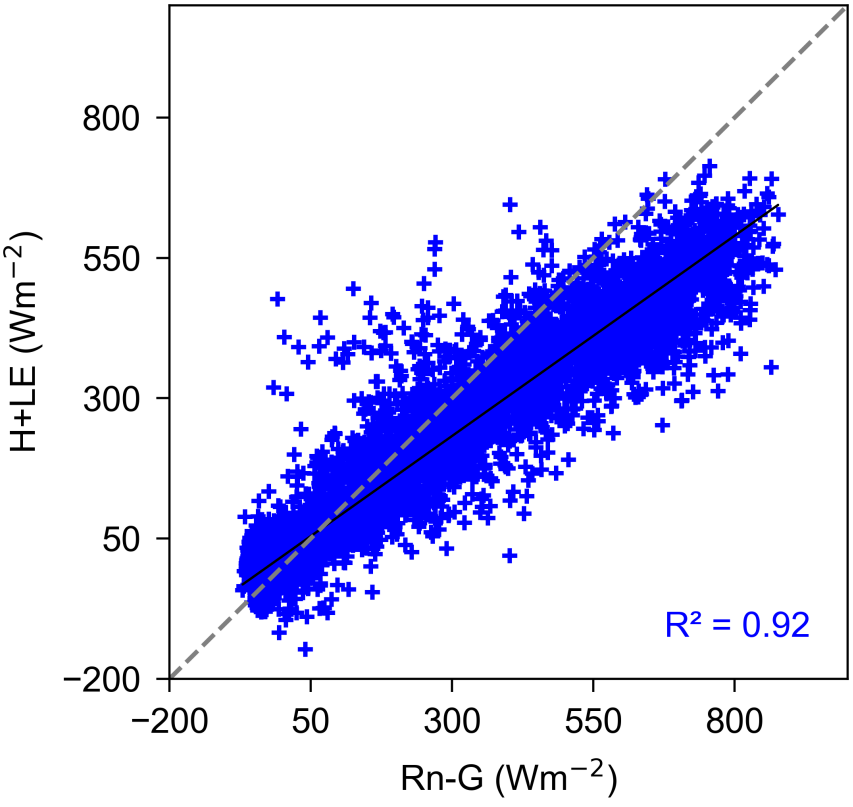

Figure A1. Scatter plot of turbulent fluxes, showing the sum of sensible and latent heat (H+LE, Wm^{-2}) plotted against available energy, defined as net radiation minus ground heat flux (Rn-G, Wm^{-2})

https://doi.org/10.5194/egusphere-2026-222
Preprint. Discussion started: 22 January 2026

Data availability. Data are available on request (katja.trachte@b-tu.de).

Author contributions. Conceptualization, data evaluation, methodology,visualization and writing the original draft, C.M. and K.T.; funding acquisition K.T.; writing–review and editing, F.P.-C.; writing–review and editing, G.C.-R.; writing–review and editing, J.H.; writing–review and editing, O.L.; writing–review and editing, A.F.; writing–review and editing, J.B. All authors have read and agreed to the published version of the manuscript.

Competing interests. The authors declare no conflicts of interest.

Acknowledgements. The authors would like to thank the Ministerio del Ambiente, Agua y Transición Ecológica (MAATE) and the Instituto Nacional de Biodiversidad de Ecuador (INABIO) for granting research permits and the foundation “Nature and Culture International” (NCI) for providing research facilities.

https://doi.org/10.5194/egusphere-2026-222
Preprint. Discussion started: 22 January 2026

References

Scikit-Learn API Reference (Stable), https://scikit-learn.org/stable/api/index.html, accessed 13 January 2026, 2026.

Ahlström, A., Raupach, M. R., Schurgers, G., Smith, B., Arneth, A., Jung, M., Reichstein, M., Canadell, J. G., Friedlingstein, P., Jain, A. K., Kato, E., Poulter, B., Sitch, S., Stocker, B. D., Viovy, N., Wang, Y. P., Wiltshire, A., Zaehle, S., and Zeng, N.: The dominant role of semi-arid ecosystems in the trend and variability of the land CO_2 sink, Science, 348, 895–899, https://doi.org/10.1126/science.aaa1668, 2015.

Baldocchi, D. D.: Assessing the eddy covariance technique for evaluating carbon dioxide exchange rates of ecosystems: past, present and future, Global Change Biology, 9, 479–492, https://doi.org/10.1046/j.1365-2486.2003.00629.x, 2003.

Barr, A., Richardson, A., Hollinger, D., Papale, D., Arain, M., Black, T., Bohrer, G., Dragoni, D., Fischer, M., Gu, L., Law, B., Margolis, H., McCaughey, J., Munger, J., Oechel, W., and Schaeffer, K.: Use of change-point detection for friction–velocity threshold evaluation in eddy-covariance studies, Agricultural and Forest Meteorology, 171-172, 31–45, https://doi.org/10.1016/j.agrformet.2012.11.023, 2013.

Bendix, J., Fries, A., Zárate, J., Trachte, K., Rollenbeck, R., Pucha-Cofrep, F., Paladines, R., Palacios, I., Orellana, J., Oñate-Valdivieso, F., et al.: RadarNet-Sur first weather radar network in tropical high mountains, Bulletin of the American Meteorological Society, 98, 1235–1254, 2017.

Bennett, A. C., Rodrigues de Sousa, T., Monteagudo-Mendoza, A., Esquivel-Muelbert, A., Morandi, P. S., Coelho de Souza, F., Castro, W., Duque, L. F., Flores Llampazo, G., Manoel dos Santos, R., et al.: Sensitivity of South American tropical forests to an extreme climate anomaly, Nature Climate Change, 13, 967–974, 2023.

Best, B. and Kessler, M.: Biodiversity and conservation in Tumbesian Ecuador and Peru, BirdLife International, Cambridge, U.K, ISBN 978-0-946888-26-9, 1995.

Biederman, J. A., Scott, R. L., Goulden, M. L., Vargas, R., Litvak, M. E., Kolb, T. E., Yepez, E. A., Oechel, W. C., Blanken, P. D., Bell, T. W., et al.: Terrestrial carbon balance in a drier world: the effects of water availability in southwestern North America, Global change biology, 22, 1867–1879, 2016.

Brienen, R. J., Phillips, O. L., Feldpausch, T. R., Gloor, E., Baker, T. R., Lloyd, J., Lopez-Gonzalez, G., Monteagudo-Mendoza, A., Malhi, Y., Lewis, S. L., et al.: Long-term decline of the Amazon carbon sink, Nature, 519, 344–348, 2015.

Calvo-Rodriguez, S., Sánchez-Azofeifa, G. A., Durán, S. M., Do Espirito-Santo, M. M., and Ferreira Nunes, Y. R.: Dynamics of carbon accumulation in tropical dry forests under climate change extremes, Forests, 12, 106, 2021.

Castellanos, E. J., Lemos, M. F., Astigarraga, L., Chacón, N., Cuvi, N., Huggel, C., Miranda, L., Moncassim Vale, M., Pierre Ometto, J., Peri, P. L., et al.: Central and south america, 2022.

Castro, S. M., Sanchez-Azofeifa, G. A., and Sato, H.: Effect of drought on productivity in a Costa Rican tropical dry forest, Environmental Research Letters, 13, 045 001, https://doi.org/10.1088/1748-9326/aaacbc, 2018.

Copernicus Global Land Service: NDVI 300 m derived from Sentinel-3 OLCI, Version 2.0.1, https://land.copernicus.eu/global/, produced by VITO NV, 2021.

Cusack, D. F., Dietterich, L. H., and Sulman, B. N.: Soil respiration responses to throughfall exclusion are decoupled from changes in soil moisture for four tropical forests, suggesting processes for ecosystem models, Global Biogeochemical Cycles, 37, e2022GB007 473, 2023.

Cuxart, J., Wrenger, B., Martínez-Villagrasa, D., Reuder, J., Jonassen, M. O., Jiménez, M. A., Lothon, M., Lohou, F., Hartogensis, O., Dünnermann, J., Conangla, L., and Garai, A.: Estimation of the advection effects induced by surface heterogeneities in the surface energy budget, Atmos. Chem. Phys., 16, 9489–9504, https://doi.org/10.5194/acp-16-9489-2016, 2016.

https://doi.org/10.5194/egusphere-2026-222
Preprint. Discussion started: 22 January 2026

Dannenberg, M. P., Smith, W. K., Zhang, Y., Song, C., Huntzinger, D. N., and Moore, D. J.: Large-scale reductions in terrestrial carbon uptake following central Pacific El Niño, Geophysical Research Letters, 48, e2020GL092 367, 2021.

Davidson, E. A. and Janssens, I. A.: Temperature sensitivity of soil carbon decomposition and feedbacks to climate change, Nature, 440, 165–173, 2006.

Del Castillo, E. G., Paw U, K. T., and Sánchez-Azofeifa, A.: Turbulence scales for eddy covariance quality control over a tropical dry forest in complex terrain, Agricultural and Forest Meteorology, 249, 390–406, https://doi.org/10.1016/j.agrformet.2017.11.014, 2018.

Dubury, A. and Duxbury, A. C.: Fundamentals of oceanography, USA: McGRAW-HILL, 1999.

Finkelstein, P. L. and Sims, P. F.: Sampling error in eddy correlation flux measurements, J. Geophys. Res., 106, 3503–3509, https://doi.org/10.1029/2000JD900731, 2001.

Foken, T., Gockede, M., Mauder, M., Mahrt, L., Amiro, B., and Munger, W.: POST-FIELD DATA QUALITY CONTROL, HANDBOOK OF MICROMETEOROLOGY.

Foken, T., Leuning, R., Oncley, S. R., Mauder, M., and Aubinet, M.: Corrections and Data Quality Control, in: Eddy Covariance, edited by Aubinet, M., Vesala, T., and Papale, D., pp. 85–131, Springer Netherlands, Dordrecht, ISBN 978-94-007-2350-4 978-94-007-2351-1, https://doi.org/10.1007/978-94-007-2351-1_4, 2012.

Fries, A., Rollenbeck, R., Bayer, F., Gonzalez, V., Onate-Valivieso, F., Peters, T., and Bendix, J.: Catchment precipitation processes in the San Francisco valley in southern Ecuador: Combined approach using high-resolution radar images and in situ observations, Meteorology and Atmospheric Physics, 126, 13–29, 2014.

García, A. G., Di Bella, C. M., Houspanossian, J., Magliano, P. N., Jobbágy, E. G., Posse, G., Fernández, R. J., and Nosetto, M. D.: Patterns and controls of carbon dioxide and water vapor fluxes in a dry forest of central Argentina, Agricultural and Forest Meteorology, 247, 520–532, https://doi.org/10.1016/j.agrformet.2017.08.015, 2017.

Garreaud, R.: Intraseasonal variability of moisture and rainfall over the South American Altiplano, Monthly Weather Review, 128, 3337–3346, 2000.

Garreaud, R. D., Vuille, M., Compagnucci, R., and Marengo, J.: Present-day south american climate, Palaeogeography, Palaeoclimatology, Palaeoecology, 281, 180–195, 2009.

Gonzalez-Valdiviezo, K., Eguiguren, P., and Homeier, J.: Variación altitudinal del contenido de carbono aéreo de bosques secos tropical en la Reserva Natural Laipuna al sur de Ecuador Altitudinal variation of aboveground carbon content of tropical dry forests in the Laipuna Nature Reserve in southern Ecuador, 2025.

González-Jaramillo, V., Fries, A., Rollenbeck, R., Paladines, J., Oñate-Valdivieso, F., and Bendix, J.: Assessment of deforestation during the last decades in Ecuador using NOAA-AVHRR satellite data, Erdkunde, pp. 217–235, https://doi.org/10.3112/erdkunde.2016.03.02, 2016.

Hammerle, A., Haslwanter, A., Schmitt, M., Bahn, M., Tappeiner, U., Cernusca, A., and Wohlfahrt, G.: Eddy covariance measurements of carbon dioxide, latent and sensible energy fluxes above a meadow on a mountain slope, Boundary-Layer Meteorol, 122, 397–416, https://doi.org/10.1007/s10546-006-9109-x, 2007.

Hiller, R., Zeeman, M. J., and Eugster, W.: Eddy-Covariance Flux Measurements in the Complex Terrain of an Alpine Valley in Switzerland, Boundary-Layer Meteorol, 127, 449–467, https://doi.org/10.1007/s10546-008-9267-0, 2008.

Humphrey, V., Berg, A., Ciais, P., Gentine, P., Jung, M., Reichstein, M., Seneviratne, S. I., and Frankenberg, C.: Soil moisture–atmosphere feedback dominates land carbon uptake variability, Nature, 592, 65–69, 2021.

https://doi.org/10.5194/egusphere-2026-222
Preprint. Discussion started: 22 January 2026

Janssen, T., Fleischer, K., Luyssaert, S., Naudts, K., and Dolman, H.: Drought resistance increases from the individual to the ecosystem level in highly diverse Neotropical rainforest: a meta-analysis of leaf, tree and ecosystem responses to drought, Biogeosciences, 17, 2621–2645, 2020.

Jarvis, P., Rey, A., Petsikos, C., Wingate, L., Rayment, M., Pereira, J., Banza, J., David, J., Miglietta, F., Borghetti, M., et al.: Drying and wetting of Mediterranean soils stimulates decomposition and carbon dioxide emission: the "Birch effect", Tree physiology, 27, 929–940, 2007.

Jolliffe, I.: Principal component analysis, in: International encyclopedia of statistical science, pp. 1094–1096, Springer, 2011.

Kljun, N., Calanca, P., Rotach, M., and Schmid, H. P.: A simple two-dimensional parameterisation for Flux Footprint Prediction (FFP), Geoscientific Model Development, 8, 3695–3713, 2015.

Loescher, H. W., Oberbauer, S. F., Gholz, H. L., and Clark, D. B.: Environmental controls on net ecosystem-level carbon exchange and productivity in a Central American tropical wet forest, Global Change Biology, 9, 396–412, https://doi.org/10.1046/j.1365-2486.2003.00599.x, 2003.

Luo, H., Oechel, W. C., Hastings, S. J., Zulueta, R., Qian, Y., and Kwon, H.: Mature semiarid chaparral ecosystems can be a significant sink for atmospheric carbon dioxide, Global Change Biology, 13, 386–396, https://doi.org/10.1111/j.1365-2486.2006.01299.x, 2007.

Malhi, Y., Nobre, A. D., Grace, J., Kruijt, B., Pereira, M. G. P., Culf, A., and Scott, S.: Carbon dioxide transfer over a Central Amazonian rain forest, J. Geophys. Res., 103, 31 593–31 612, https://doi.org/10.1029/98JD02647, 1998.

Matzinger, N., Andretta, M., Gorsel, E. V., Vogt, R., Ohmura, A., and Rotach, M. W.: Surface radiation budget in an Alpine valley, Quarterly Journal of the Royal Meteorological Society: A journal of the atmospheric sciences, applied meteorology and physical oceanography, 129, 877–895, 2003.

Mauder, M., Cuntz, M., Drüe, C., Graf, A., Rebmann, C., Schmid, H. P., Schmidt, M., and Steinbrecher, R.: A strategy for quality and uncertainty assessment of long-term eddy-covariance measurements, Agricultural and Forest Meteorology, 169, 122–135, https://doi.org/10.1016/j.agrformet.2012.09.006, 2013.

Mendes, K. R., Campos, S., Da Silva, L. L., Mutti, P. R., Ferreira, R. R., Medeiros, S. S., Perez-Marin, A. M., Marques, T. V., Ramos, T. M., De Lima Vieira, M. M., Oliveira, C. P., Gonçalves, W. A., Costa, G. B., Antonino, A. C. D., Menezes, R. S. C., Bezerra, B. G., and Santos E Silva, C. M.: Seasonal variation in net ecosystem CO2 exchange of a Brazilian seasonally dry tropical forest, Scientific Reports, 10, 9454, https://doi.org/10.1038/s41598-020-66415-w, 2020.

Mendes, K. R., Oliveira, P. E., Lima, J. R. S., Moura, M. S., Souza, E. S., Perez-Marin, A. M., Cunha, J. E. B., Mutti, P. R., Costa, G. B., de Sá, T. N. M., et al.: The caatinga dry tropical forest: A highly efficient carbon sink in South America, Agricultural and Forest Meteorology, 369, 110 573, 2025.

Miles, L., Newton, A. C., DeFries, R. S., Ravilious, C., May, I., Blyth, S., Kapos, V., and Gordon, J. E.: A global overview of the conservation status of tropical dry forests, Journal of biogeography, 33, 491–505, 2006.

Moore, C. J.: Frequency response corrections for eddy correlation systems, Boundary-Layer Meteorol, 37, 17–35, https://doi.org/10.1007/BF00122754, 1986.

Murkute, C., Sayeed, M., Pucha-Cofrep, F., Carrillo-Rojas, G., Homeier, J., Limberger, O., Fries, A., Bendix, J., and Trachte, K.: Turbulent Energy and Carbon Fluxes in an Andean Montane Forest—Energy Balance and Heat Storage, Forests, 15, https://doi.org/10.3390/f15101828, 2024.

https://doi.org/10.5194/egusphere-2026-222
Preprint. Discussion started: 22 January 2026

Nie, C., Huang, Y., Zhang, S., Yang, Y., Zhou, S., Lin, C., and Wang, G.: Effects of soil water content on forest ecosystem water use efficiency through changes in transpiration/evapotranspiration ratio, Agricultural and Forest Meteorology, 308-309, 108 605, https://doi.org/10.1016/j.agrformet.2021.108605, 2021.

NOAA Climate Prediction Center: ENSO: El Niño/La Niña Overview and Monitoring, https://www.cpc.ncep.noaa.gov/products/analysis_monitoring/enso_advisory/, accessed 12 January 2026, 2024.

Novick, K., Walker, J., Chan, W., Schmidt, A., Sobek, C., and Vose, J.: Eddy covariance measurements with a new fast-response, enclosed-path analyzer: Spectral characteristics and cross-system comparisons, Agricultural and Forest Meteorology, 181, 17–32, https://doi.org/10.1016/j.agrformet.2013.06.020, 2013.

Novick, K. A., Ficklin, D. L., Grossiord, C., Konings, A. G., Martínez-Vilalta, J., Sadok, W., Trugman, A. T., Williams, A. P., Wright, A. J., Abatzoglou, J. T., et al.: The impacts of rising vapour pressure deficit in natural and managed ecosystems, Plant, Cell & Environment, 47, 3561–3589, 2024.

Papale, D., Reichstein, M., Aubinet, M., Canfora, E., Bernhofer, C., Kutsch, W., Longdoz, B., Rambal, S., Valentini, R., Vesala, T., and Yakir, D.: Towards a standardized processing of Net Ecosystem Exchange measured with eddy covariance technique: algorithms and uncertainty estimation, Biogeosciences, 3, 571–583, https://doi.org/10.5194/bg-3-571-2006, 2006.

Paw U, K. T., Baldocchi, D. D., Meyers, T. P., and Wilson, K. B.: Correction of eddy-covariance measurements incorporating both advective effects and density fluxes, Boundary-Layer Meteorology, 97, 487–511, 2000.

Portillo-Quintero, C. A. and Sánchez-Azofeifa, G. A.: Extent and conservation of tropical dry forests in the Americas, Biological conservation, 143, 144–155, 2010.

Poulter, B., Frank, D., Ciais, P., Myneni, R. B., Andela, N., Bi, J., Broquet, G., Canadell, J. G., Chevallier, F., Liu, Y. Y., Running, S. W., Sitch, S., and van der Werf, G. R.: Contribution of semi-arid ecosystems to interannual variability of the global carbon cycle, Nature, 509, 600–603, https://doi.org/10.1038/nature13376, 2014.

Pucha-Cofrep, D., Peters, T., and Bräuning, A.: Wet season precipitation during the past century reconstructed from tree-rings of a tropical dry forest in Southern Ecuador, Global and Planetary Change, 133, 65–78, https://doi.org/10.1016/j.gloplacha.2015.08.003, 2015.

Reichstein, M., Falge, E., Baldocchi, D., Papale, D., Aubinet, M., Berbigier, P., Bernhofer, C., Buchmann, N., Gilmanov, T., Granier, A., Grunwald, T., Havrankova, K., Ilvesniemi, H., Janous, D., Knohl, A., Laurila, T., Lohila, A., Loustau, D., Matteucci, G., Meyers, T., Miglietta, F., Ourcival, J.-M., Pumpanen, J., Rambal, S., Rotenberg, E., Sanz, M., Tenhunen, J., Seufert, G., Vaccari, F., Vesala, T., Yakir, D., and Valentini, R.: On the separation of net ecosystem exchange into assimilation and ecosystem respiration: review and improved algorithm, Global Change Biol, 11, 1424–1439, https://doi.org/10.1111/j.1365-2486.2005.001002.x, 2005.

Restrepo-Coupe, N., Campos, K. S., Alves, L. F., Longo, M., Wiedemann, K. T., de Oliveira Jr, R. C., Aragao, L. E., Christoffersen, B. O., Camargo, P. B., Figueira, A. M. S., et al.: Contrasting carbon cycle responses to dry (2015 El Niño) and wet (2008 La Niña) extreme events at an Amazon tropical forest, Agricultural and Forest Meteorology, 353, 110 037, 2024.

Rodda, S. R., Thumaty, K. C., Praveen, M., Jha, C. S., and Dadhwal, V. K.: Multi-year eddy covariance measurements of net ecosystem exchange in tropical dry deciduous forest of India, Agricultural and Forest Meteorology, 301-302, 108 351, https://doi.org/10.1016/j.agrformet.2021.108351, 2021.

Rojas-Robles, N. E., Garatuza-Payán, J., Álvarez-Yépiz, J. C., Sánchez-Mejía, Z. M., Vargas, R., and Yépez, E. A.: Environmental controls on carbon and water fluxes in an old-growth tropical dry forest, Journal of Geophysical Research: Biogeosciences, 125, e2020JG005 666, 2020.

https://doi.org/10.5194/egusphere-2026-222
Preprint. Discussion started: 22 January 2026

Rollenbeck, R., Orellana-Alvear, J., Bendix, J., Rodriguez, R., Pucha-Cofrep, F., Guallpa, M., Fries, A., and Celleri, R.: The Coastal El Niño event of 2017 in Ecuador and Peru: A weather radar analysis, Remote Sensing, 14, 824, 2022.

Siyum, Z. G.: Tropical dry forest dynamics in the context of climate change: syntheses of drivers, gaps, and management perspectives, Ecological Processes, 9, 1–16, 2020.

Spannl, S., Volland, F., Pucha, D., Peters, T., Cueva, E., and Bräuning, A.: Climate variability, tree increment patterns and ENSO-related carbon sequestration reduction of the tropical dry forest species Loxopterygium huasango of Southern Ecuador, Trees, 30, 1245–1258, https://doi.org/10.1007/s00468-016-1362-0, 2016.

Stan, K. and Sanchez-Azofeifa, A.: Tropical Dry Forest Diversity, Climatic Response, and Resilience in a Changing Climate, Forests, 10, 443, https://doi.org/10.3390/f10050443, 2019.

Tan, Z.-H., Zhang, Y.-P., Deng, X.-B., Song, Q.-H., Liu, W.-J., Deng, Y., Tang, J.-W., Liao, Z.-Y., Zhao, J.-F., Song, L., et al.: Interannual and seasonal variability of water use efficiency in a tropical rainforest: Results from a 9 year eddy flux time series, Journal of Geophysical Research: Atmospheres, 120, 464–479, 2015.

Trachte, K.: Atmospheric Moisture Pathways to the Highlands of the Tropical Andes: Analyzing the Effects of Spectral Nudging on Different Driving Fields for Regional Climate Modeling, Atmosphere, 9, 456, https://doi.org/10.3390/atmos9110456, 2018.

Turnipseed, A. A., Anderson, D. E., Burns, S., Blanken, P. D., and Monson, R. K.: Airflows and turbulent flux measurements in mountainous terrain, Agricultural and Forest Meteorology, 125, 187–205, https://doi.org/10.1016/j.agrformet.2004.04.007, 2004.

Vickers, D. and Mahrt, L.: Quality Control and Flux Sampling Problems for Tower and Aircraft Data, J. Atmos. Oceanic Technol., 14, 512–526, https://doi.org/10.1175/1520-0426(1997)014<0512:QCAFSP>2.0.CO;2, 1997.

Vuille, M., Franquist, E., Garreaud, R., Lavado Casimiro, W. S., and Cáceres, B.: Impact of the global warming hiatus on Andean temperature, Journal of Geophysical Research: Atmospheres, 120, 3745–3757, 2015.

Wang, L., Jiao, W., MacBean, N., Rulli, M. C., Manzoni, S., Vico, G., and D'Odorico, P.: Dryland productivity under a changing climate, Nature Climate Change, 12, 981–994, 2022.

Webb, E. K., Pearman, G. I., and Leuning, R.: Correction of flux measurements for density effects due to heat and water vapour transfer, Quart J Royal Meteoro Soc, 106, 85–100, https://doi.org/10.1002/qj.49710644707, 1980.

Werner, F. A. and Homeier, J.: Diverging Elevational Patterns of Tree vs. Epiphyte Species Density, Beta Diversity, and Biomass in a Tropical Dry Forest, Plants, 13, 2555, 2024.

Wharton, S., Schroeder, M., Paw U, K. T., Falk, M., and Bible, K.: Turbulence considerations for comparing ecosystem exchange over old-growth and clear-cut stands for limited fetch and complex canopy flow conditions, Agricultural and Forest Meteorology, 149, 1477–1490, https://doi.org/https://doi.org/10.1016/j.agrformet.2009.04.002, 2009.

Whiteman, C. D., Allwine, K. J., Fritschen, L. J., Orgill, M. M., and Simpson, J. R.: Deep valley radiation and surface energy budget microclimates. Part I: Radiation, Journal of Applied Meteorology and Climatology, 28, 414–426, 1989.

Wilczak, J. M., Oncley, S. P., and Stage, S. A.: Sonic Anemometer Tilt Correction Algorithms, Boundary-Layer Meteorology, 99, 127–150, https://doi.org/10.1023/A:1018966204465, 2001.

Wu, J., Su, Y., Chen, X., Liu, L., Yang, X., Gong, F., Zhang, H., Xiong, X., and Zhang, D.: Leaf shedding of Pan-Asian tropical evergreen forests depends on the synchrony of seasonal variations of rainfall and incoming solar radiation, Agricultural and Forest Meteorology, 311, 108 691, 2021.

https://doi.org/10.5194/egusphere-2026-222
Preprint. Discussion started: 22 January 2026

Wutzler, T., Lucas-Moffat, A., Migliavacca, M., Knauer, J., Sickel, K., Šigut, L., Menzer, O., and Reichstein, M.: Basic and extensible post-processing of eddy covariance flux data with REddyProc, Biogeosciences, 15, 5015–5030, https://doi.org/10.5194/bg-15-5015-2018, 2018.

Xing, Y., Wang, P., Zhang, D., Sun, H., and Li, S.: Convergent control of soil temperature on seasonal carbon flux in Tibetan alpine meadows: An in-situ monitoring study, Ecological Indicators, 156, 111 116, https://doi.org/10.1016/j.ecolind.2023.111116, 2023.

Zeng, Y., Liu, Y., Hong, P., He, P., and Ma, J.: Main environmental driver and seasonality of water use efficiency in tropical forests, Journal of Hydrology, 654, 132 944, 2025.

Zhang, Y., Song, C., Sun, G., Band, L. E., Noormets, A., and Zhang, Q.: Understanding moisture stress on light use efficiency across terrestrial ecosystems based on global flux and remote-sensing data, Journal of Geophysical Research: Biogeosciences, 120, 2053–2066, 2015.